LTV REPORT NO. 3-32300/5CR-9
ARPA ORDER NO. 4320

Photon Avalanche Laser Improvement Program

LTV AEROSPACE AND DEFENSE COMPANY
VOUGHT MISSILES AND ADVANCED PROGRAMS DIVISION
P. O. BOX 650003
DALLAS, TEXAS 75265-0003

DTIC
S ECTE D
DEC 0 5 1985
D

NOVEMBER 1985

FINAL REPORT FOR PERIOD NOVEMBER 1983 - MAY 1985

APPROVED FOR PUBLIC RELEASE; DISTRIBUTION UNLIMITED

SPONSORED BY:

DEFENSE ADVANCED RESEARCH PROJECTS AGENCY
1400 WILSON BLVD.
ARLINGTON, VA 22209

LTV Aerospace and Defense
Vought Missiles and
Advanced Programs Division

DTIC FILE COPY

12 2 164

Blank page

SECURITY CLASSIFICATION OF THIS PAGE (When Data Entered)

REPORT DOCUMENTATION PAGE		READ INSTRUCTIONS BEFORE COMPLETING FORM
1. REPORT NUMBER 3-32300/5CR-9	2. GOVT ACCESSION NO.	3. RECIPIENT'S CATALOG NUMBER
4. TITLE (and Subtitle) PHOTON AVALANCHE LASER IMPROVEMENT PROGRAM		5. TYPE OF REPORT & PERIOD COVERED FINAL REPORT 11-83 - 11-84
		6. PERFORMING ORG. REPORT NUMBER R-93000/3P-4
7. AUTHOR(s) M. E. KOCH		8. CONTRACT OR GRANT NUMBER(s) N00014-84-C-2019 ARPA ORDER NO. 4320
9. PERFORMING ORGANIZATION NAME AND ADDRESS LTV AEROSPACE AND DEFENSE COMPANY VOUGHT MISSILES AND ADVANCED PRORAMS DIVISION P. O. BOX 650003, DALLAS, TEXAS 75265-0003		10. PROGRAM ELEMENT, PROJECT, TASK AREA & WORK UNIT NUMBERS
11. CONTROLLING OFFICE NAME AND ADDRESS DEFENSE ADVANCED RESEARCH PROJECTS AGENCY 1400 WILSON BLVD. ARLINGTON, VA 22209		12. REPORT DATE DECEMBER 1984
		13. NUMBER OF PAGES
14. MONITORING AGENCY NAME & ADDRESS(if different from Controlling Office) NAVAL RESEARCH LABORATORY 4555 OVERLOOK AVE., S. W. WASHINGON, DC 20375		15. SECURITY CLASS. (of this report) UNCLASSIFIED
		15a. DECLASSIFICATION/DOWNGRADING SCHEDULE

16. DISTRIBUTION STATEMENT (of this Report)

APPROVED FOR PUBLIC RELEASE; DISTRIBUTION UNLIMITED

17. DISTRIBUTION STATEMENT (of the abstract entered in Block 20, if different from Report)

18. SUPPLEMENTARY NOTES

19. KEY WORDS (Continue on reverse side if necessary and identify by block number)

INFRARED LASER; PHOTON AVALANCHE; RARE-EARTH; PRASEODYMIUM, Lanthanum Chloride.

20. ABSTRACT (Continue on reverse side if necessary and identify by block number)

The main thrust of this program was to increase the output power and efficiency of a photon avalanche laser demonstrated in an earlier and related program (Contract #N00014-82-C-2631 & P00001). However, material problems plagued the effort from the outset. Identification and solution of these problems has led to an enormous increase in production yield of Pr doped $LaCl_3$ laser crystals as well as the discovery of a contaminate →next pg

DD FORM 1473 1 JAN 73   EDITION OF 1 NOV 65 IS OBSOLETE
S/N 0102-LF-014-6601

which needs to be eliminated in future work. Overall, an increase in laser power output has not achieved, but new insights may lead to large payoffs in the near future. Keywords: → to field (19)

PHOTON AVALANCHE LASER IMPROVEMENT PROGRAM

FINAL REPORT

REPORT NO. 3-32300/5CR-9

Prepared by: M. E. Koch

Sponsored by

The views and conclusions contained in this document are those of the authors
and should no be interpreted as necessarily representing the official policies,
either expressed or implied of the defense advanced research projects agency or
the U. S. Government.

LTV AEROSPACE AND DEFENSE COMPANY
VOUGHT MISSILES AND ADVANCED PROGRAMS DIVISION
P. O. BOX 650003
DALLAS, TEXAS 75265-0003

CONTENTS

1.0 INTRODUCTION

The primary thrust of this program was to increase output power and efficiency of the photon avalanche laser, first demonstrated in December 1982 during a previous and related program (Contract #N00014-82-C-2631 & P00001). Additionally, growth of new crystals was anticipated to support experimental work in several other areas, including: (1) a comparison of transversely and longitudinally pumped laser configurations; (2) a measurement of gain region extent; (3) an investigation of laser and avalanche fluorescence transient response. The attainment of these goals was frustrated at the outset by materials production problems. Eventually, adjustment in cooldown gradient for the freeze cycle of the Bridgeman growth process led to an astounding increase in growth yields over previously obtainable levels. The crystals were of higher optical quality than previous crystals but they did not yield laser action. Spectral evidence indicates a new channel in these crystals for de-exitation of ions, potentially leading to an increase in the critical pump intensity needed to establish the photon avalanche and a corresponding increase in the pump intensity threshold for lasing. Although it cannot be ruled out, it is not likely that the loss of laser operation was due simply to a change in the production process but to rather another problem, namely, an uncontrolled LaOCl contamination level. This problem will be addressed in the near future. In the work reported here, new issues have been uncovered whose resolution may lead to the desired breakthrough in output laser power.

In advance of discussions detailing contract results, it is appropriate to briefly highlight here relevant theory, predictions, and sample preparation technology.

1.1 BACKGROUND

The photon avalanche process was discovered at Vought Corporation Advanced Technology Center (ATC) in 1975.[1] Various aspects of the process have been explored experimentally,[2] and an analytical model has been created.[3] Several predictions from the model have been corroborated in experiments, including infrared lasing.[4]

An infrared-to-visible unconversion process in Pr^{3+} is shown relative to energy-level spacing in Figure 1-1.[5] During a typical experiment, the $^3H_5$ metastable level is excited by signal radiation near 4.5 µm. Further excitation from $^3H_5$ to $^3P_1$ is provided by the green output of a cw dye laser, fluorescence from the $^3P_0 \rightarrow ^3H_6$ and $^3P_1 \rightarrow ^3F_2$ transitions or from $^3P_0 \rightarrow ^3F_2$ is detected by a photomultiplier tube in conjunction with suitable collection optics and filters. At temperatures from 20 to 300K, fluorescence is mostly at red wavelengths.

A plot of fluorescence output versus pump power is shown in Figure 1-2 for a $LaBr_3$:Pr crystal at 230 K and laser pumped from $^3H_5(2)$ to $^3P_1(1)$. More than a two-orders-of-magnitude increase in output occurs at a well-defined pump intensity P_c, referred to here as the critical pump for onset of avalanche. Below P_c, output is linear with both infrared input power and pump power, consistent with other work and as expected from the usual theory of upconveresion. Above P_c, output is essentially insensitive to infrared excitation and highly nonlinear with pump intensity.

In a separate experiment, it has been observed that part of the absorbed pump power reappears as infrared radiation near 4.5 µm. Generation of this radiation by decay of $^3H_6$ followed by ground-state reabsorption could, in principle, feed an avalanche process. If so, about 1-10 mW/cm^2 of infrared flux would be required to account for avalanche fluorescence. This amount of radiation is not consistent with the low fluorescence efficiency ($\sim 10^{-20}$cm^2) for $^3H_5 \leftarrow ^3H_4$ photon absorption.

The resonance condition on pump wavelength and the nonlinear dependence of fluorescence on pump intensity suggest that the avalanche derives from a multiple pump photon absorption process involving the $^3H_5$ level. A mechanism to create a $^3H_5$ population via pump excitation is diagrammed in Figure 1-3. Pr^{3+} ion A is initially in the $^3H_6$ state via upconversion from $^3H_5$ to $^3P_1$ followed by fluorescence relaxation to $^3H_6$. Subsequently, ion A decays from $^3H_6$ to $^3H_5$, transferring the transition energy to a nearby Pr ion B and activating it from $^3H_4$ to $^3H_5$. The result is two ions in the $^3H_5$ state available for excitation and further buildup of the $^3H_5$ population. From this picture it follows that the heavy pump absorption in the avalanche region originates with an excited state, and implies a large excited-state population.
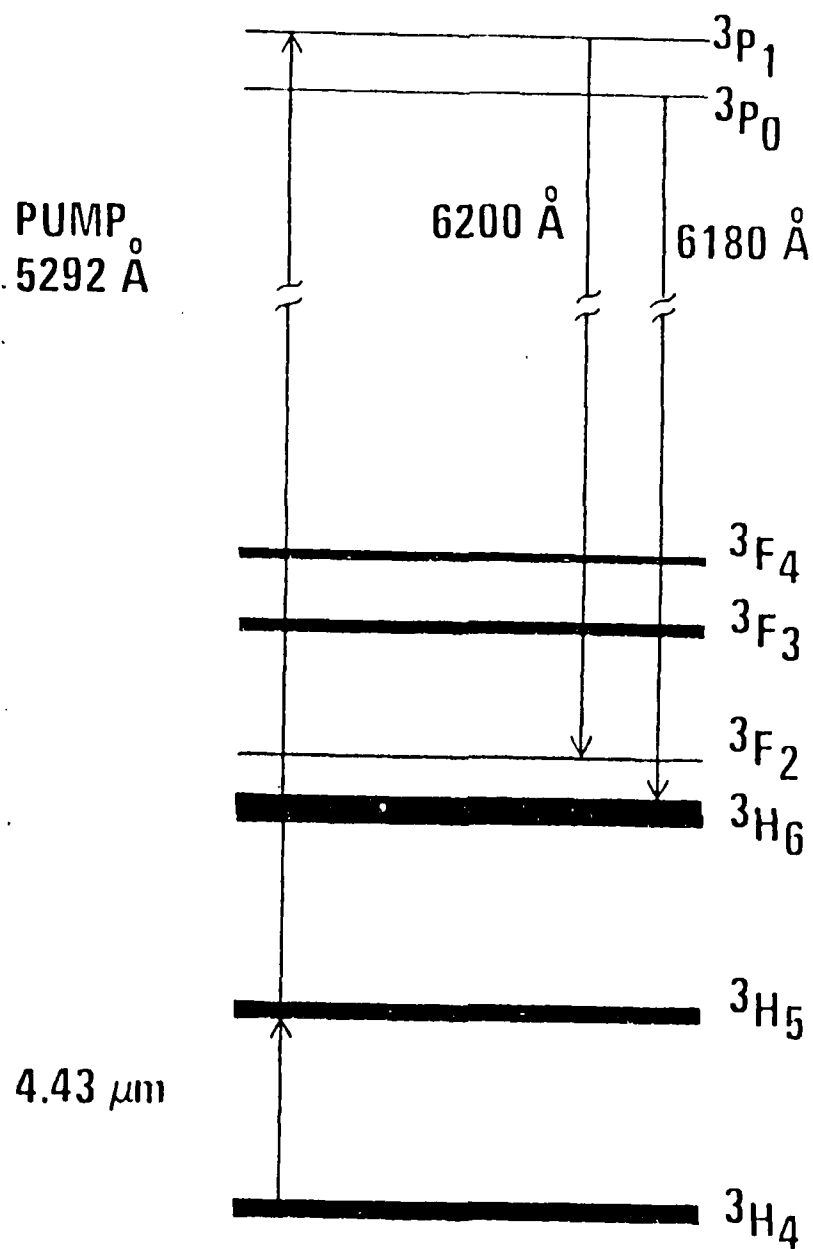
2

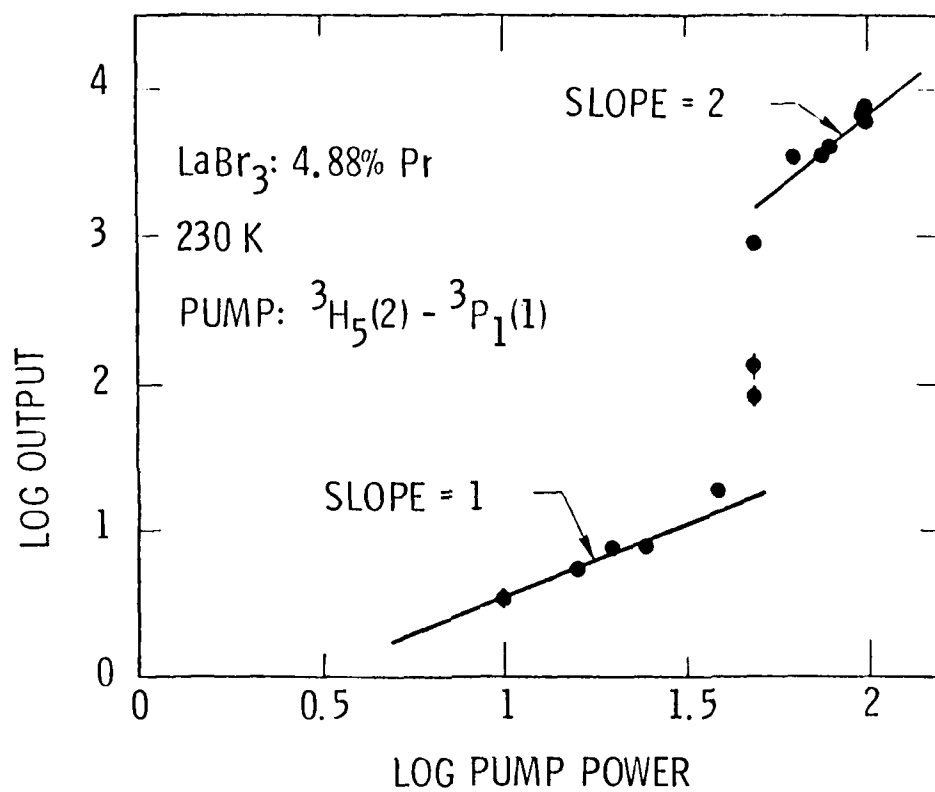Figure 1-1. Partial Energy Level Diagram of $LaCl_3$:Pr Showing the Relevant Upconversion Scheme

3

Figure 1-2. Fluorescence Output of Pr^{3+} vs. Incident Pump Power in the Vicinity of the Critical Pump Power Flux
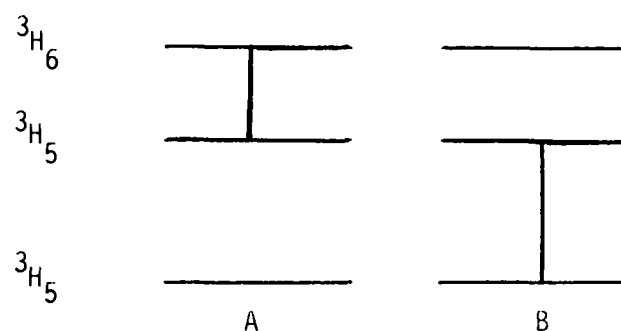
$^3H_6$

$^3H_5$

$^3H_5$

A   B

Figure 1-3. Ion-Pair Resonant Energy Transfer between Two Pr^{3+} Ions

The idea of energy transfer between neighboring Pr^{3+} ions has been used as the basis for a new nonlinear theory of upconversion.[3] In effect, linear rate equations for the upconversion process were suitably modified to include the ion pair relaxation mechanism, described above. The first order steady state solution is

$$S_0 = c_2 \; P \; [[(P/P_c - 1)^2 + C_1 \; F_s]^{1/2} + (P/P_c - 1)]$$ (1)

where S_0 is fluorescence output (arbitrary units), c_1 and c_2 are constants (definable in terms of relaxation rates, fluorescence efficiency, cross-sections for pump and infrared absorption, etc.), P is the pump flux (watts/cm^2), and F_s is the infrared signal flux (watts/cm^2); pump flux and signal flux are applied uniformly to the same region of the crystal.

In contrast to the usual steady-state solution of the linear theory, Equation (1) provides the possibility of a non-zero output even if $F_s = 0$, i.e., $S_0 = c_2 P \; (P/P_c - 1)$. Obviously, $P \geq P_c$ must hold. This condition leads naturally to the identification of P_c as a critical pump flux.

1.2 PUMP ABSORPTION

Resonant excitation of a Pr^{3+} ion between an infrared electronic level (2) and a higher optical level (5) removes energy from the pump beam. The decrease in pump flux in a distance dx along the beam is given by

$$dP = -\sigma_p \; P(n_2 - n_5) \; dx,$$ (2)

where σ_p is the cross-section/ion for the 2-5 transition, and n_2 and n_5 are the number of Pr ions per unit volume in levels 2 ($^2H_5$) and 5 ($^3P_1$).

For the usual IRQC experiment at low values of pump power ($P \ll P_c$), the occupation probability of the infrared level is proportional to infrared flux and independent of pump power. In addition, $n_5 \ll n_2$ so that the absorption coefficient is constant at a relatively small value. If consideration is given to the pump range $P > P_c$, where the metastable population depends on pump power and pump absorption is no longer negligible, Equation (2) becomes

$$dP/dx - -\beta \, P \, (P / P_c -1), \qquad (3)$$

where β^{-1} is a second-order polynomial in pump flux. An estimate for the pump-independent terms is $\sim$50 micrometers. Retaining only this term in Equation (3) results in the solution

$$f = P/P_c,$$

$$f(x) - f(o)/[f(o)(1-\exp(-\beta x)) + (-\beta x)] \qquad (4)$$

Figure 1-4 is a prediction for relative pump power variation with distance into a Pr-based crystal. It is clear that a long absorption distance tends to limit the emerging pump flux to the critical value, $P(\infty) = P_c$.

1.3 POPULATION INVERSION

An infrared laser near 4.5 μm was predicted from the avalanche model and now verified with Pr-doped $LaCl_3$. The required population inversion is a feature of the avalanche region for modest increases in optical pumping above the critical pump rate. Figure 1-5 shows the expected dependence of occupation probabilities for levels $^3H_4$ and $^3H_6$ and the ground state $^3H_4$ vs. the normalized pump parameter P/P_c. Given a suitable arrangement of external mirror for optical feedback, several lasing transitions become possible if $P > 3 \, P_c$; $^3H_6 \to \, ^3H_5$ and/or $^3H_5 \to \, ^3H_4$ in the 4.3 - 5.3 μm region; and possibly $^3H_6 \to \, ^3H_4$ in the 2.1 - 2.7 μm region; and possibly $^3F_3 \to \, ^3H_4$ at 1.6 μm.
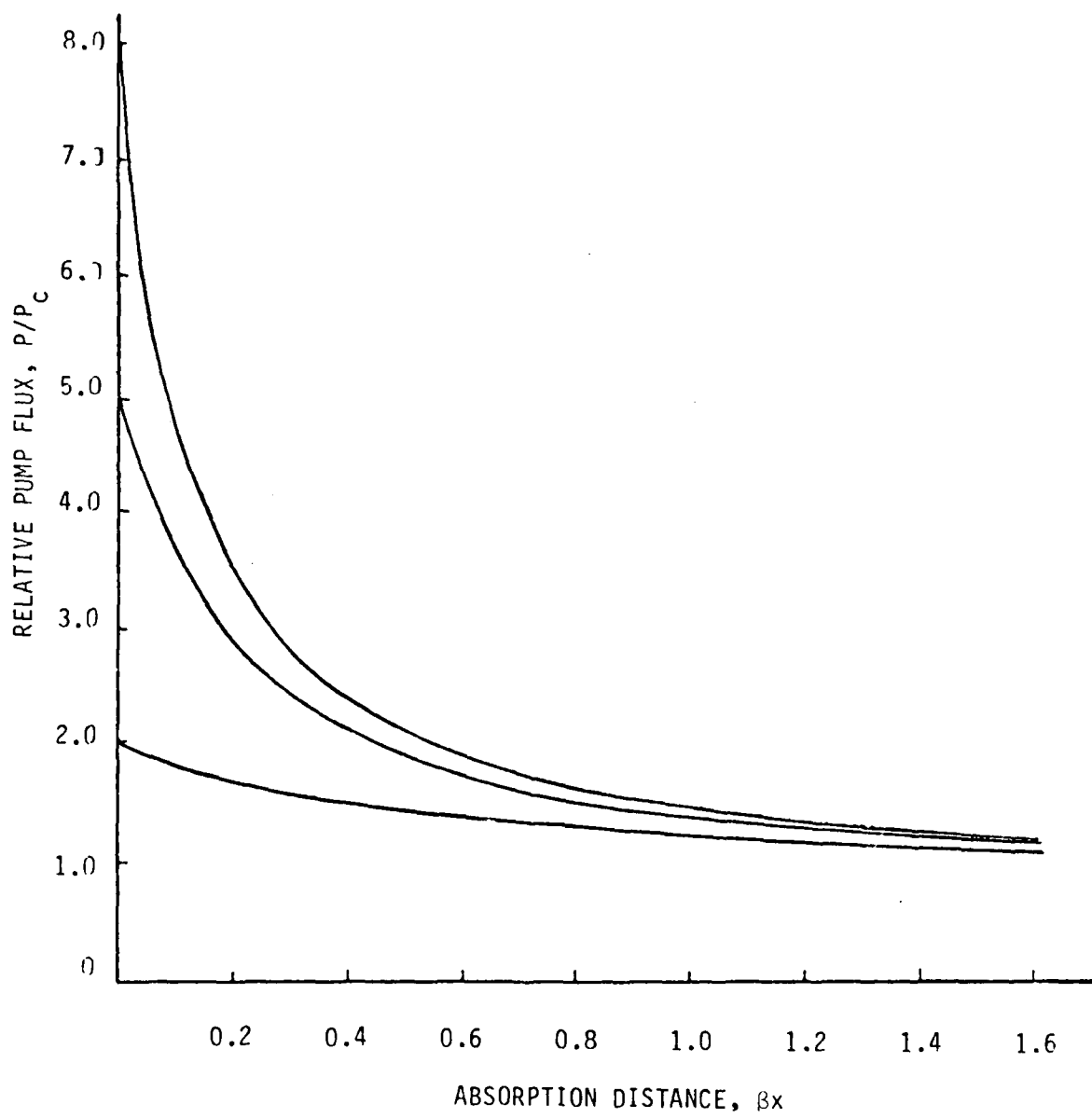
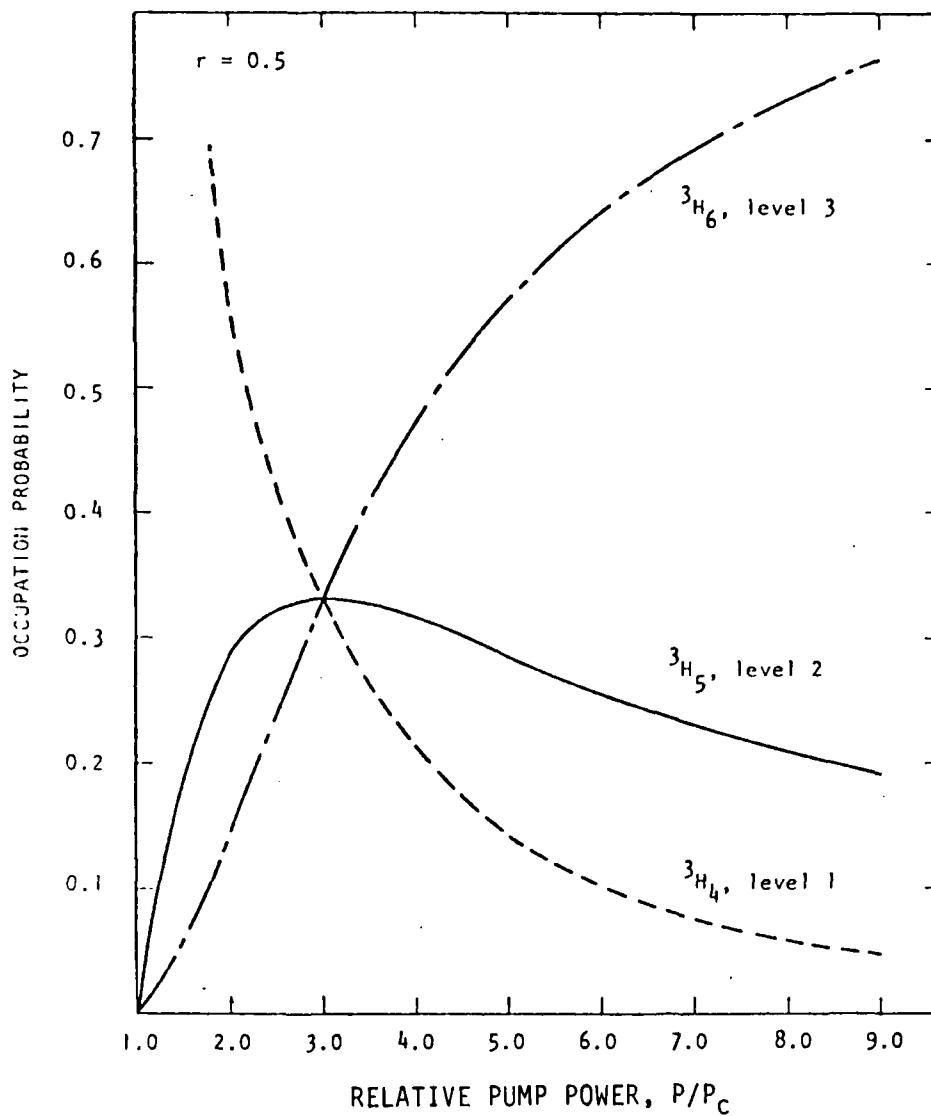Figure 1-4. Predicted Pump Absorption in the Avalanche Region

Figure 1-5. Predicted Population Inversion in LaCl$_3$:Pr

The expected small signal gain coefficient for the $^3H_6 \rightarrow {}^3H_5$ transition depends on system parameters and relative pump flux as:

$$g_0 = n\,\sigma\,[r\,(P/P_c - 1) - 1](P/P_c - 1)/(r^{-1} + (P/P_c - 1)[1 + r\,(P/P_c - 1)]), \quad (5)$$

where n is the number of Pr ions/cm^3, σ is the cross-section for absorption of infrared photons, and r is a combination of spontaneous lifetimes for the $^3H_6 \rightarrow {}^3H_5$ transition (τ_{32}), and the $^3H_6 \rightarrow {}^3H_4$ transition (τ_{31}), vis.,

$$r = (2/\tau_{31} + 1/\tau_{32})^{-1}/\tau_m.$$

The lifetimes of $^3H_5$ and $^3H_6$ have been measured at low Pr concentration (0.001 percent) and 77°K to be $\tau_m = 22$ msec and $\tau_3 = \tau_{31} + \tau_{32} = 15$ msec. Therefore, the system parameter r is in the range 0.36 ($\tau_{32} = \infty$) to 0.73 ($\tau_{31} = \infty$). Other relevant parameters are $\sigma \sim 2 \times 10^{-20}$ cm^2 and $n \sim 1 \times 10^{20}$ ions/cm^3 for each 1 percent of Pr concentration. As an example, consider the specifications r = 0.5, 3 percent concentration Pr, and $P = 6 P_c$. These values imply a high gain coefficient $g_0 = 2.3$ cm^{-1}.

A high gain coefficient is consistent with the laser demonstration experiments reported in later sections. However, a quantitative measure of g_0 has not been possible to date.

1.4 SAMPLE FABRICATION TECHNOLOGY

An extensive technology for crystal growth and sample preparation was developed at LTV's Advanced Technology Center in the early 1970s. A description of the technology utilized for this program is presented in the following discussion, especially appropriate in view of recent technology improvements.

A flow diagram outlining the crystal growth process is shown in Figure 1-6 and referenced in following paragraphs.

$PrCl_3$ and $LaCl_3$ powders were obtained from Research Chemicals Corporation (Phoenix) at the highest purity level (99.999 percent). At our laboratory these powders are predried in a vacuum oven, pumped by a liquid nitrogen trapped roughing pump at 423°K for eight hours and then placed in the dry box
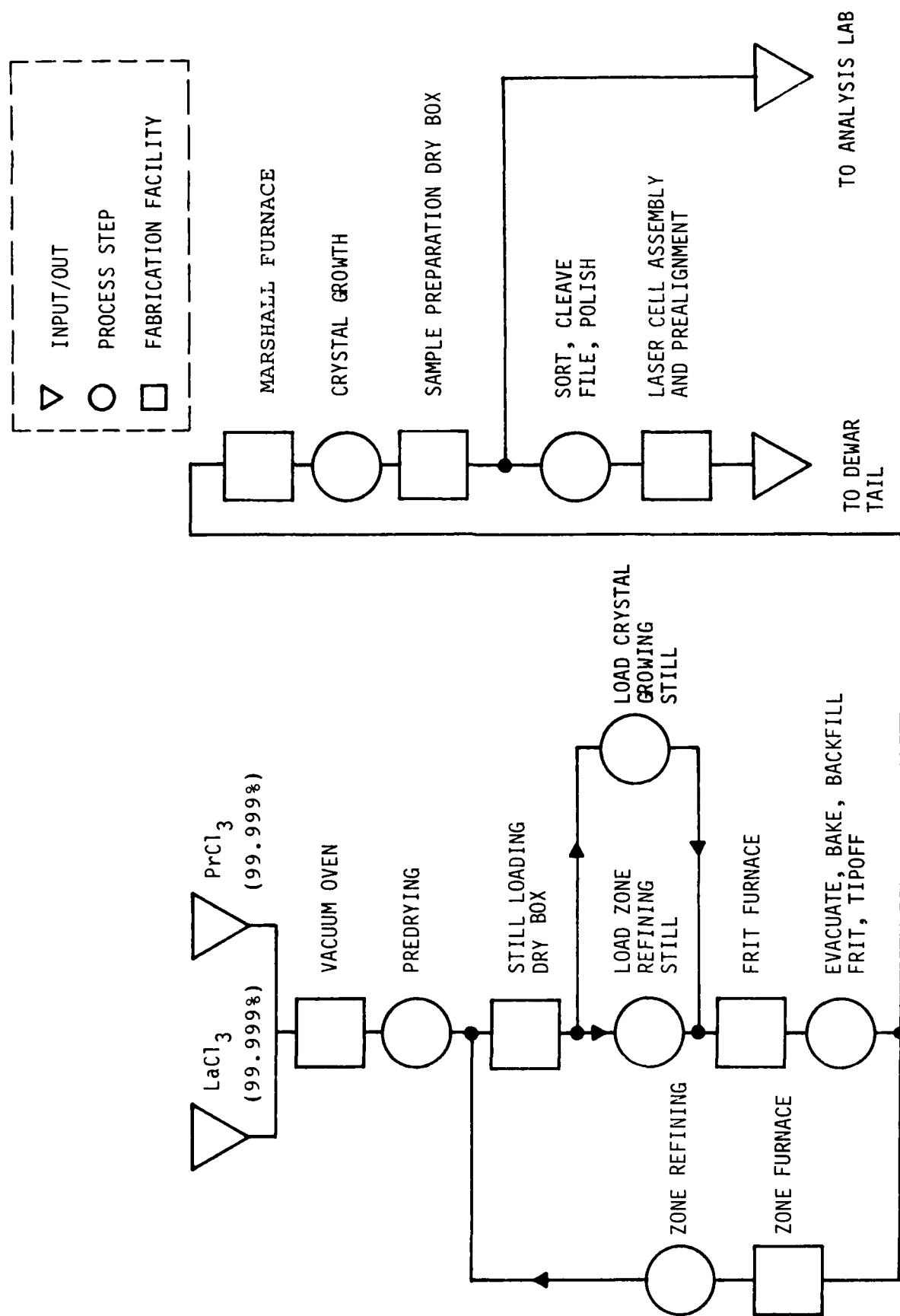
Figure 1-6. Materials Processing Flow Diagram

10

for storage and loading into distillation cells (stills). Two types of quartz still are used, namely, zone refining and crystal growth stills. These are identical except that the latter has a small capillary tube attached at the bottom (Figure 1-7). A fritting process is used to prepare powder materials for both zone refining and crystal pulling. The powders (initial material or zone refined material) are loaded in the dry box into the end of the still opposed to the pumping port. The still is then removed from the dry box to the frit furnace station. Here it is held with the pumping and material holding arms at a small incline to the table, with the pump arm lower. The arm containing the frit followed by the ampoule is held in a nearly vertical position. An oven is placed about the material arm and the powder is sublimed and condensed in the still near the vertical arm opening. After removing the oven, the material is melted with a torch and then flows down the vertical tube to the frit. A frit furnace is placed around the vertical arm, the material melted, and the still backfilled with Ar gas to press the melt through the frit into the ampoule. The ampole is then tipped off and taken to the zone refining or crystal pulling furnaces. The crystal pulling furnaces are shown in Figure 1-8.

Zone refining takes two days during which a cylindrical oven is cycled back and forth over the ampoule 10 times. The oven is turned on for one direction in each cycle driving impurities to one end of the ampoule. After this step the ampoule is taken back to the dry box and broken, and a portion from the purer end removed for use. The refined $PrCl_3$ and $LaCl_3$ are weighed and mixed in a desired proportion and placed in a crystal growth still.

The crystal growth still is processed at the frit furnace station as described above. The growth ampoule is then attached to a quartz rod and lowered into the crystal growth oven, capillary tube down, via a clock motor. For the purpose of this discussion the oven can be described as having two zones. The upper zone is hot enough to ensure complete melting of the material while the lower zone is held below the freezing point. As the ampoule passes from the upper to the lower zone, the material melts and then freezes. The freezing takes place first in the capillary tube and here crystal growth is forced to begin (Bridgeman Process). This melt-freeze sequence takes 144 hours with an additional 60 hours for cooling the crystal ampoule to room temperature. At
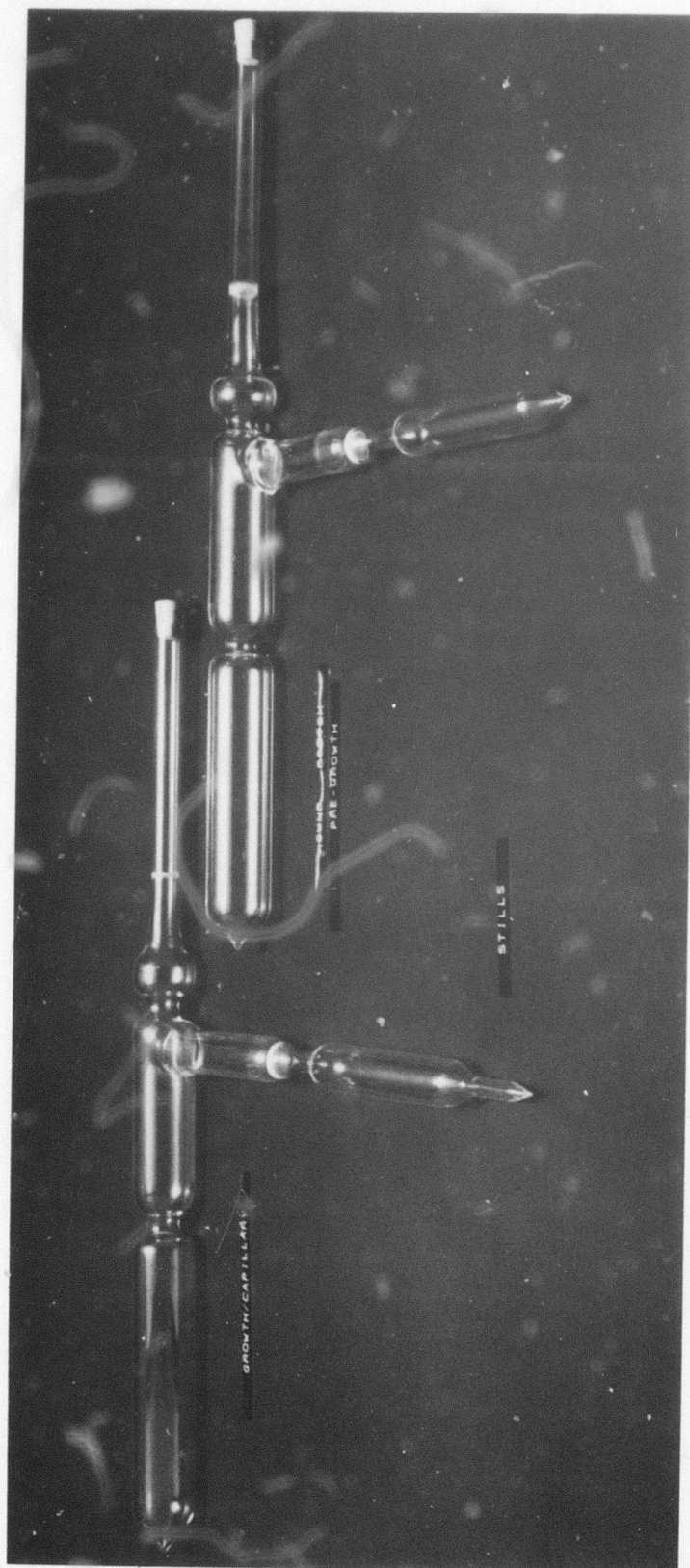
11

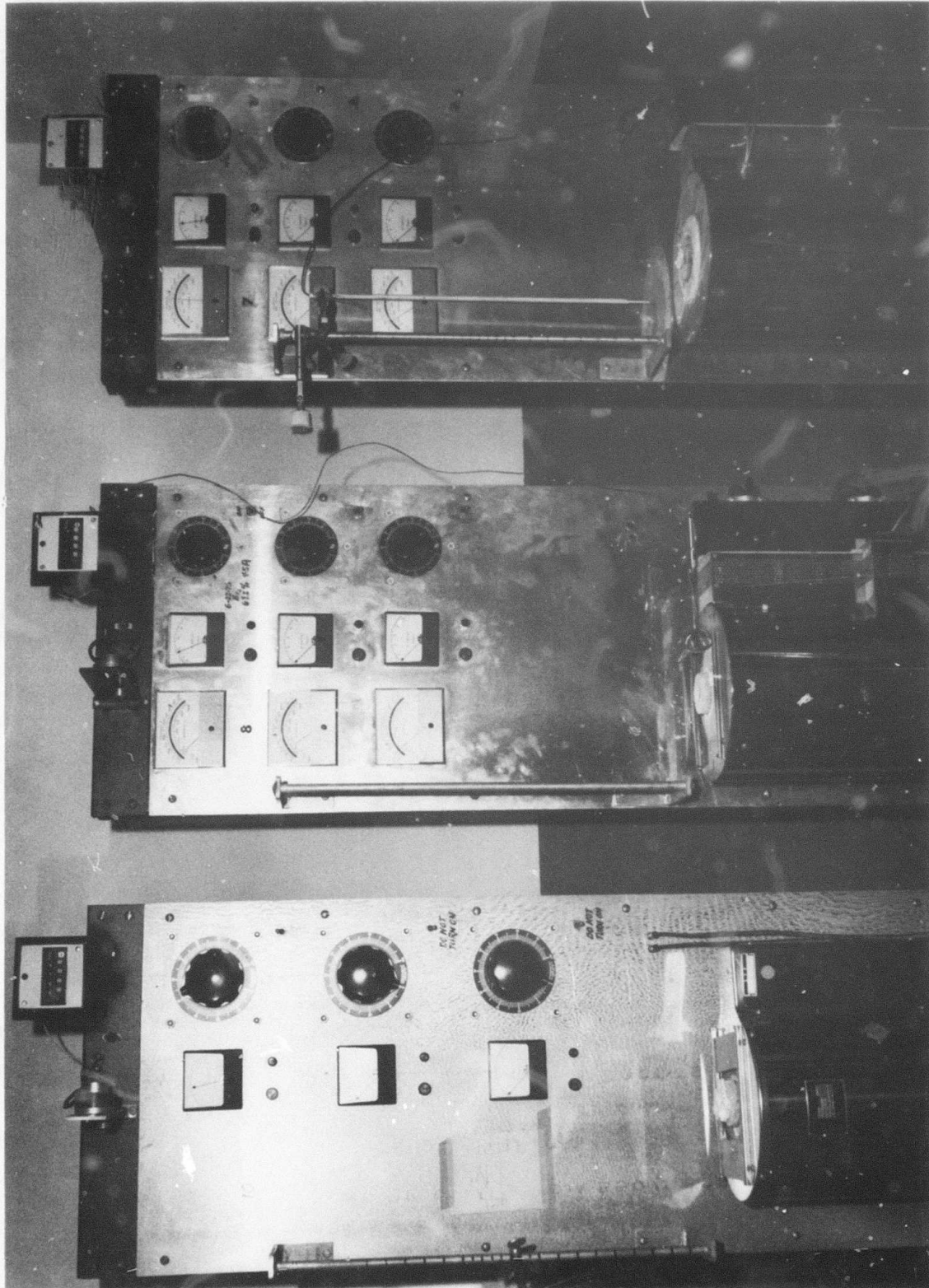Figure 1-7. Quartz Distillation Cells (Stills)

Figure 1-8. Crystal Pulling Furnaces

13

this point the ampoule is placed in the sample preparation dry box and broken.
Generally the boule is cracked throughout with a few large sections of single
crystal material included. These sections are cataloged with respect to
orientation to the capillary tube which is itself usually parallel to the
symmetry axis of the crystal. Orientation has been verified by placing the
sample between crossed polarizers and examining the throughput of a diverging
light beam. A small piece of the boule is sent to an analysis laboratory for a
determination of the percent by weight of La and Pr. The crystals remain in
the dry box until needed for experimentation.

The orientation of a crystal selected for an experiment is certified by
finding two cleavage planes (these are parallel to the symmetry axis). It is
then sawed and filed into roughly the desired shape. The final step is
polishing on beeswax laps with increasingly fine grades of polishing compound,
ending with 0.3 micron allumina. A finished crystal is shown in Figure 1-9.
After polishing, the crystal is placed in a sealed transfer cell and taken to
the laser cell assembly and alignment dry box. Here it is positioned in a
sample mounting block (Figure 1-10) and referenced to the final position in the
dewar tail. An appropriate sample cell (Figure 1-11) is sealed with indium to
the sample mounting block, and the assembly is then taken to the laser
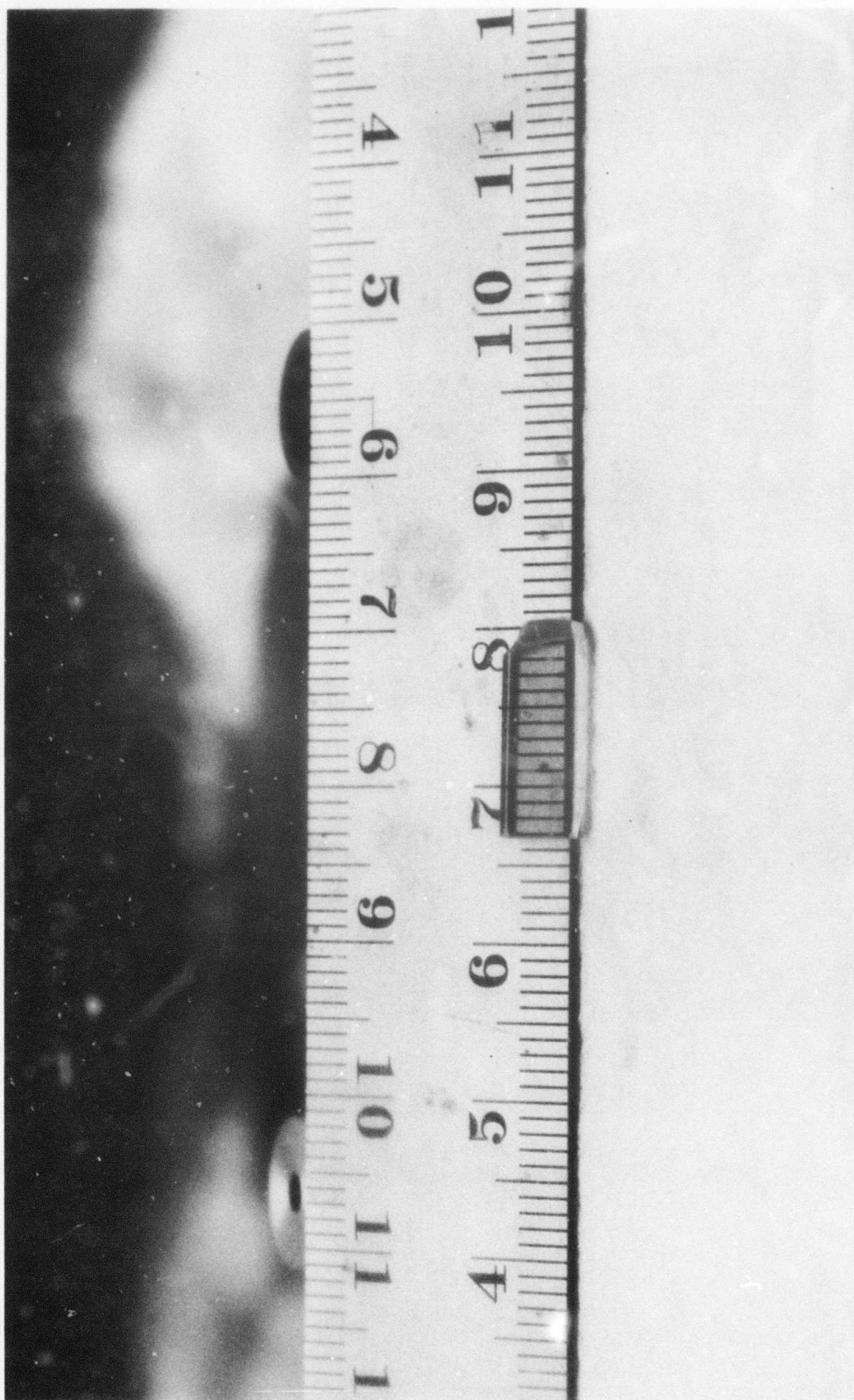laboratory, mounted in the dewar tail and cooled to 77K (nominal).
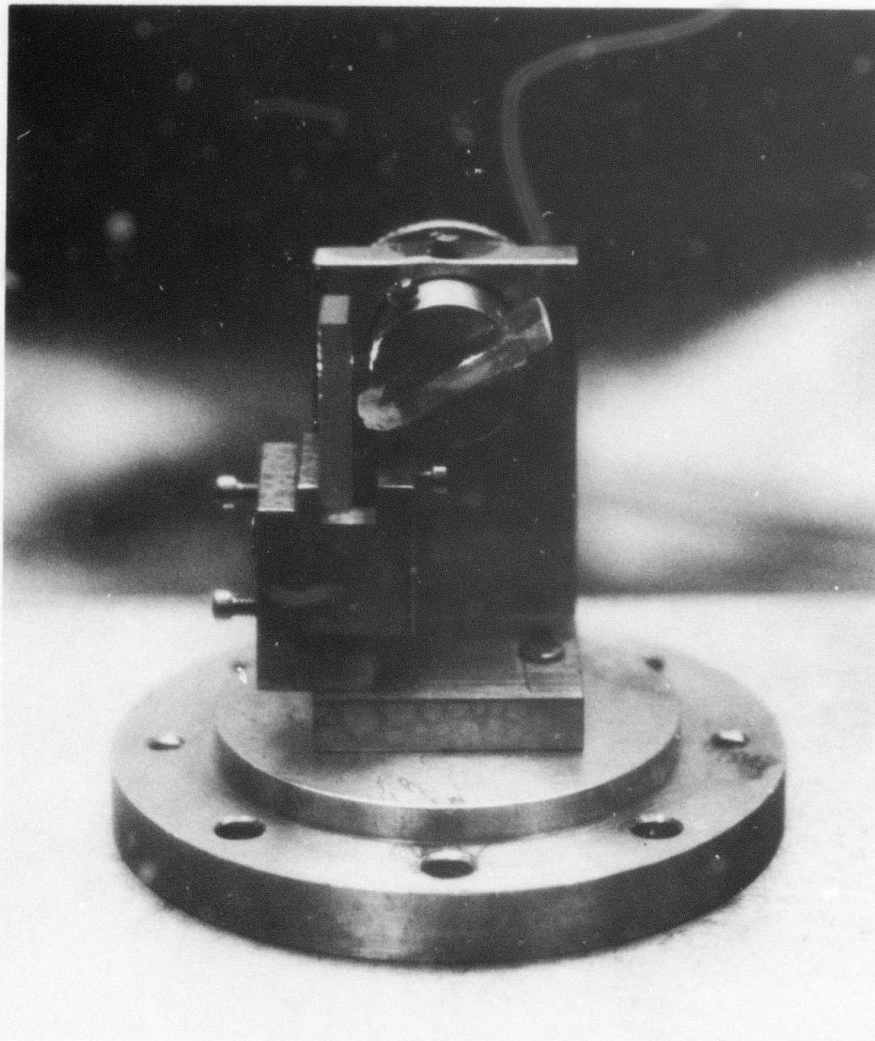
Figure 1-9. Polished Crystal

15

Figure 1-10.   Sample Mounting Block - Laser Crystal at Brewster's
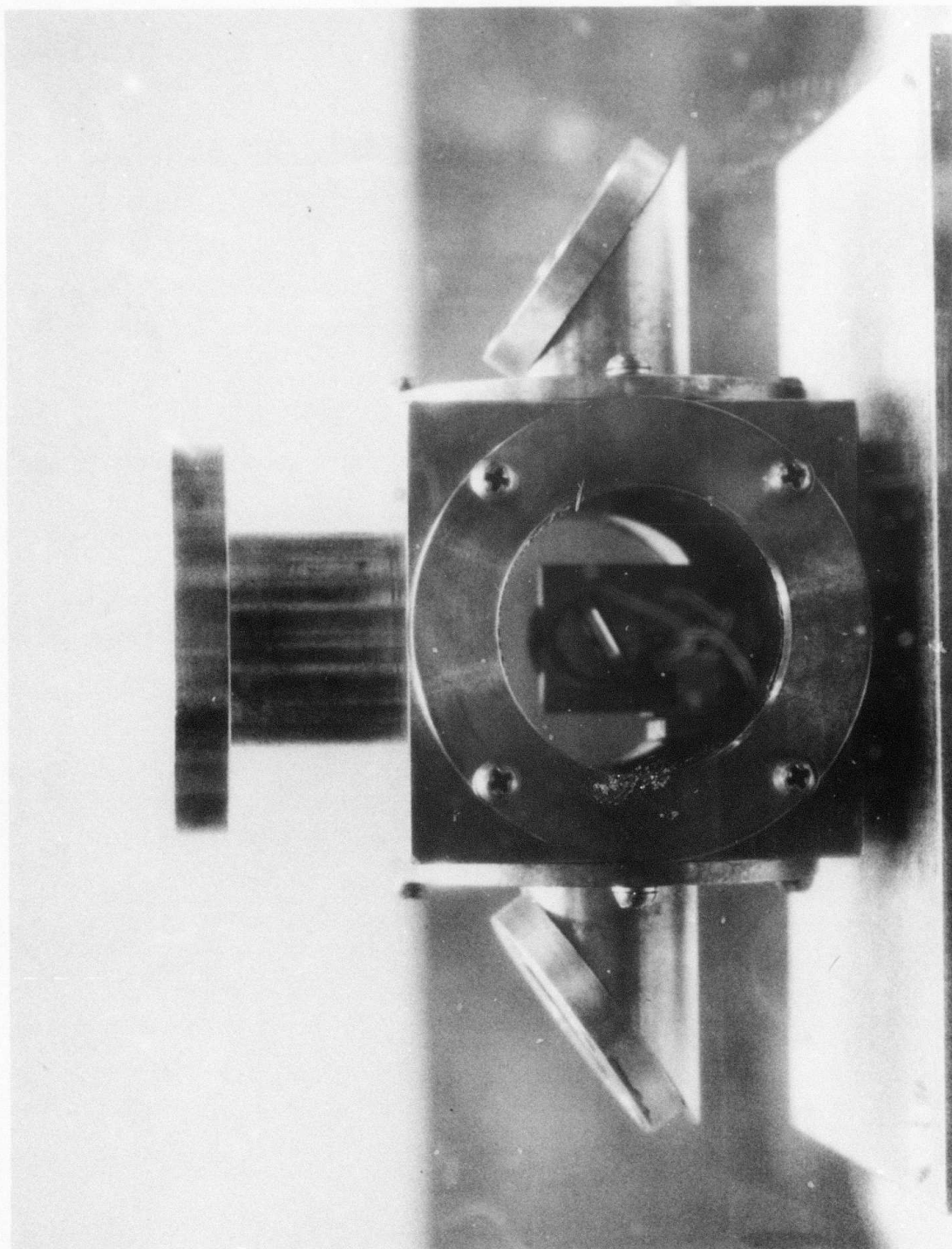Angle, Flat Mirror Perpendicular to Table.

Figure 1-11. Sample Cell

2.0 PHOTON AVALANCHE LASER DEVELOPMENT PROGRAM (PAL1) RESULTS

The work reported here extends results of a program started in October, 1981 (N00014-82-C-2631 & P00001). It is natural therefore to summarize the results of the previous program in order to place this work in perspective.

2.1 PHOTON AVALANCHE CHARACTERIZATION STUDIES

Prior to a laser experiment an investigation of selected photon avalanche properties was conducted. These characterization studies are grouped into four categories: preliminary studies, scattering loss, spectroscopic data, and the modulated population experiment.

2.1.1 Preliminary Studies

Initial efforts in the laboratory were aimed at investigating infrared output vs. pump intensity, and pump experiments were performed with a 2.1 percent by weight Pr doped crystal. The pump laser was tuned to the π $^3P_1(1)$ - $^3H_5$ (2) line (529.2 nm) and the beam was oriented perpendicular to the crystal axis. The fluorescence detected was emitted perpendicular to both the optic axis and the pump beam direction. A calcium flouride collection lens was used lens was used to obtain a detectable signal in the infrared. The infrared detector was a 1 mm x 1 mm InSb diode used in the photoconductive mode and amplified by a Perry amplifier (Model 750). This detector was used in all (except where noted) later experiments for sensing infrared radiation. A PMT was used to detect visible emission. The pump beam was chopped at 5 Hz and synchronous detection was used via a lock-in amplifier for all signals.

Figure 2-1 shows the dependence of infrared (4-5 μm) fluorescence on pump power. The sharp onset as well as the linear dependence of the fluorescence on pump power is consistent with theoretical predictions. Another result of the experiment was the observation that crystal fluorescence with σ-line pumping parallel to the crystal axis is comparable in strength to fluorescence with π-line pumping orthogonal to the crystal axis.
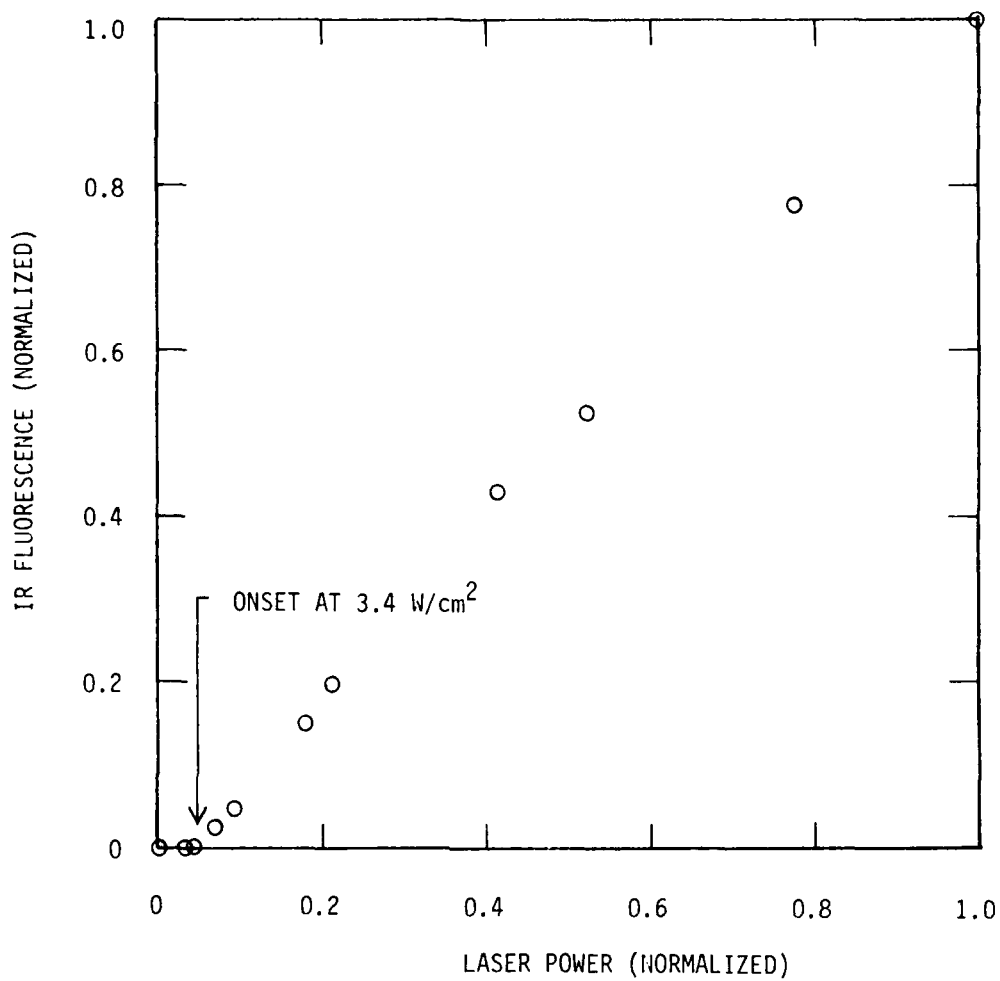
Figure 2-1. Avalanche IR (4 → 5 μm) Output vs Laser Power

In a second experiment, three samples of differing concentrations were pumped via the π line while the avalanche fluorescence was detected normal to the pump laser beam and the crystal by means of an imaging system. A pinhole was placed in front of the detector, in this case a PMT, and together these were translated through the image plane of the avalanche, allowing a determination of avalanche penetration depth into the crystal. The pump laser was operated at 30 mW and focused with a 50 cm fl lens. The results shown in Figure 2-2 indicate greater penetration at smaller concentrations with a 3.7 percent crystal allowing nearly twice the penetration of 7.4 percent crystal. The 3.7 percent concentration crystal also yielded over three times the infrared signal of the 7.4 percent crystal. A .53 percent crystal yielded about the same infrared signal as the 3.6 percent but much larger penetration. On the basis of these results the 3 percent concentration was selected as a reasonable starting base for the laser experiments. Criteria for a better choice were not developed since it was planned to examine the effects of concentration vs cavity parameters after the laser demonstration.

2.1.2 Scattering Loss

At the outset of the previous contract, the transmission losses for light propagating through the crystals reported by earlier workers caused great concern. Volume scattering was suspected as the most significant loss mechanism by observation of visible laser beams passed through the crystals. The degree of scattering has been found in this work to depend on the direction of the laser beam relative to the symmetry axis. Visible light scattering at 632.8 nm is reduced with the beam parallel rather than perpendicular to the crystals symmetry axis. A hypothesis emerged that the scattering was due to small fissures oriented lengthwise along the optic axis. A few electron micrographs were taken and revealed a somewhat striated material.

An experiment was set up to measure the transmission of the crystal in the infrared compared to that in the visible. For this purpose a HeNe laser at 632.8 nm and one at 3.39 μm were overlapped and focused in the center of the crystal. The transmission of each laser was monitored with a thermopile at the opposite side of the dewar tail. Results are shown in Figure 2-3. The transmission loss in the infrared is consistent with Fresnel reflection losses calculated for both crystal surfaces using the index of refraction, 1.7. The
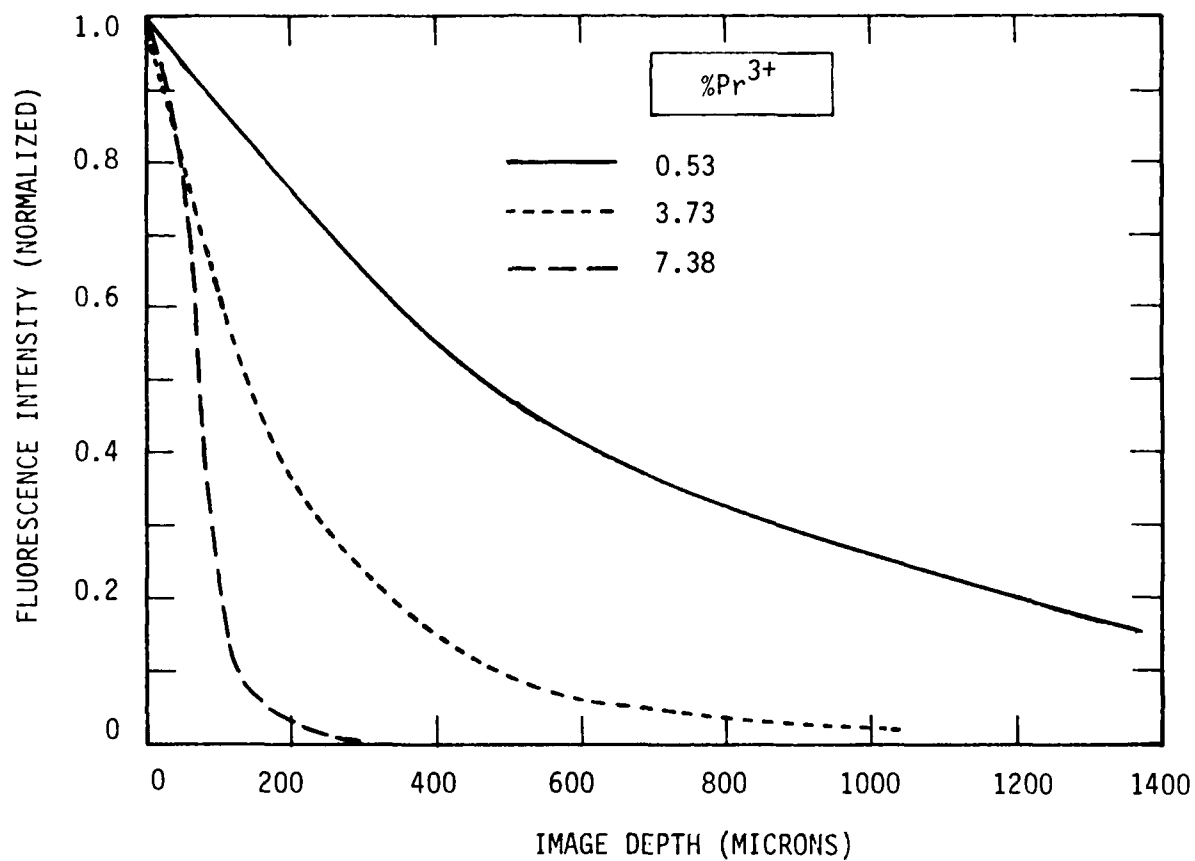
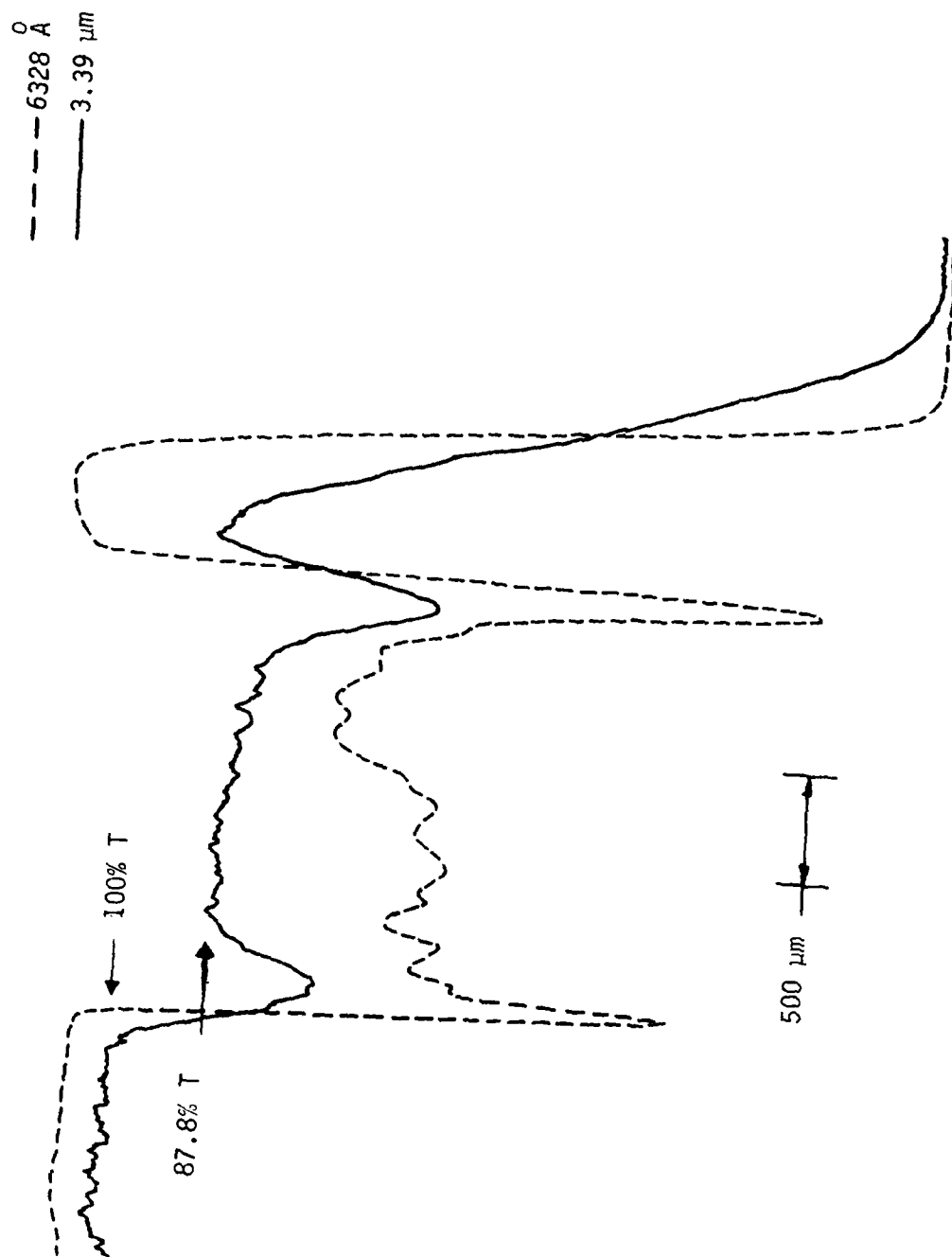Figure 2-2. Penetration of Focused Laser-Distance Measured From
Crystal Face

21

Figure 2-3 Transmission of a Focussed Laser Beam Through Pr Doped LaCl₃ -
Crystal Translated Across the Focus of the Laser Beam

evidence shows that the scattering losses are insignificant in the infrared and do not represent a problem for lasing.

2.2 Modulated Population Experiment

The avalanche model described earlier predicts significant depopulation of the Pr ion ground state. To test for this radical change of state an experiment was devised which allowed the population of the ground state to be monitored in a small region while the surrounding crystal was driven into avalanche. This experiment exploits the near overlap of the Ar+ pump laser line at 488.0 nm with the $^3P_0(0) \leftarrow ^3H_4(2)$ transition at 488.26 nm. The relevant energy levels for the population measurement experiment are shown in Figure 2-4. The experimental arrangement is shown in Figure 2-5. A small fraction of the 488.0 nm laser beam was chopped and used to excite the $^3P_0(0) \leftarrow ^3H_4(2)$ transition. Fluorescence from the $^3P_0-^3H_6$ transition was synchronously detected with a PMT through a 1/4 meter monochrometer and then amplified by a lock-in amplifier. Assuming the population of the $^3P_0$ level to be much less than the $^3H_4$ level population, the signal obtained is proportional to the ground state population. The crystal used was 3.23 percent molar Pr concentration, polished to a thickness of 0.48 mm. Care was taken to reduce the probe laser intensity to a level which did not significantly alter the fluorescence induced by the pump laser.

The avalanche effect was found to be accompanied by significant depopulation of the ground state ions. The fluorescence signal routinely fell to 30-45 percent of the zero pump value. However, a major error in this experiment is due to scattering of probe laser light, causing the probe laser to sample a section of the crystal larger than the pumped volume. The measured change in population is therefore a conservatively valued lower limit.

The ground state population decreases with pump intensity as shown in Figure 2-6. The population decrease saturates above 60 mW. It is possible that the $^3H_4$ states are nearly 100 percent depopulated for these pump powers through the entire crystal. Transmission of the pump laser through the crystal as a function of pump power was also monitored. The results are shown in Figure 2-7. The resulting hysteresis curve is characteristic of optical bistability phenomena. It is created by continuously raising and lowering and then raising the pump intensity.
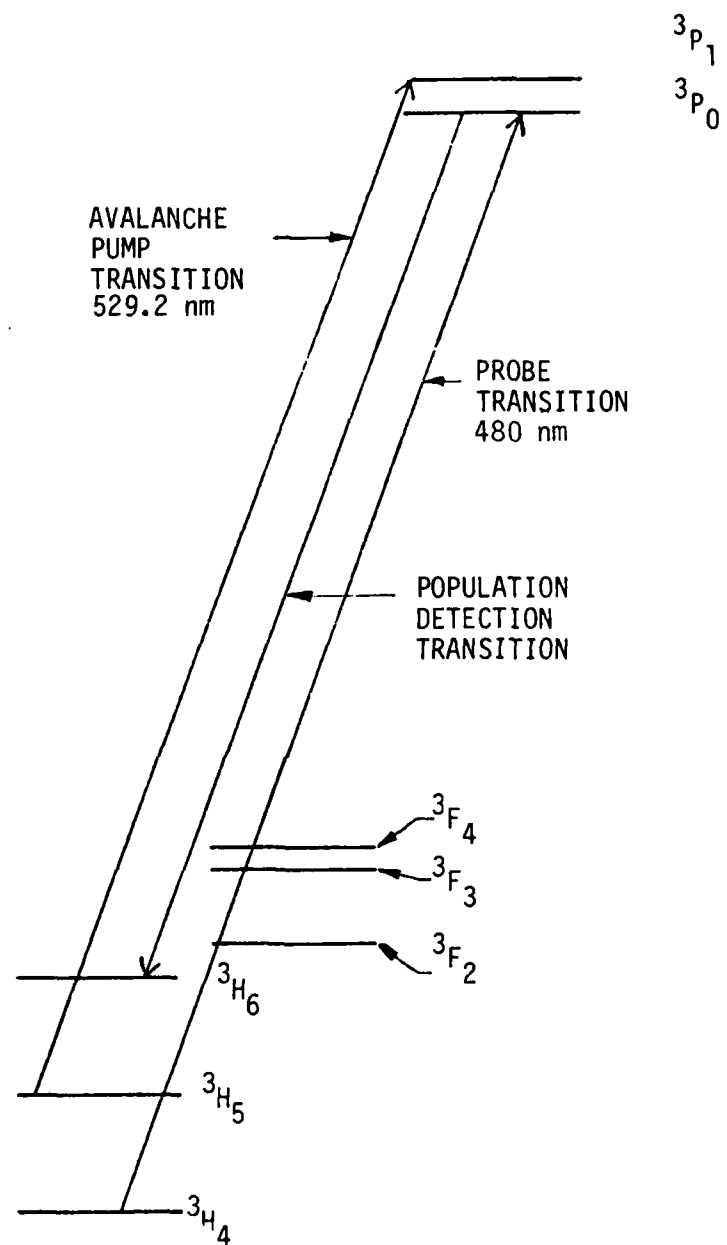
Figure 2-4. Modulated Population Measurement

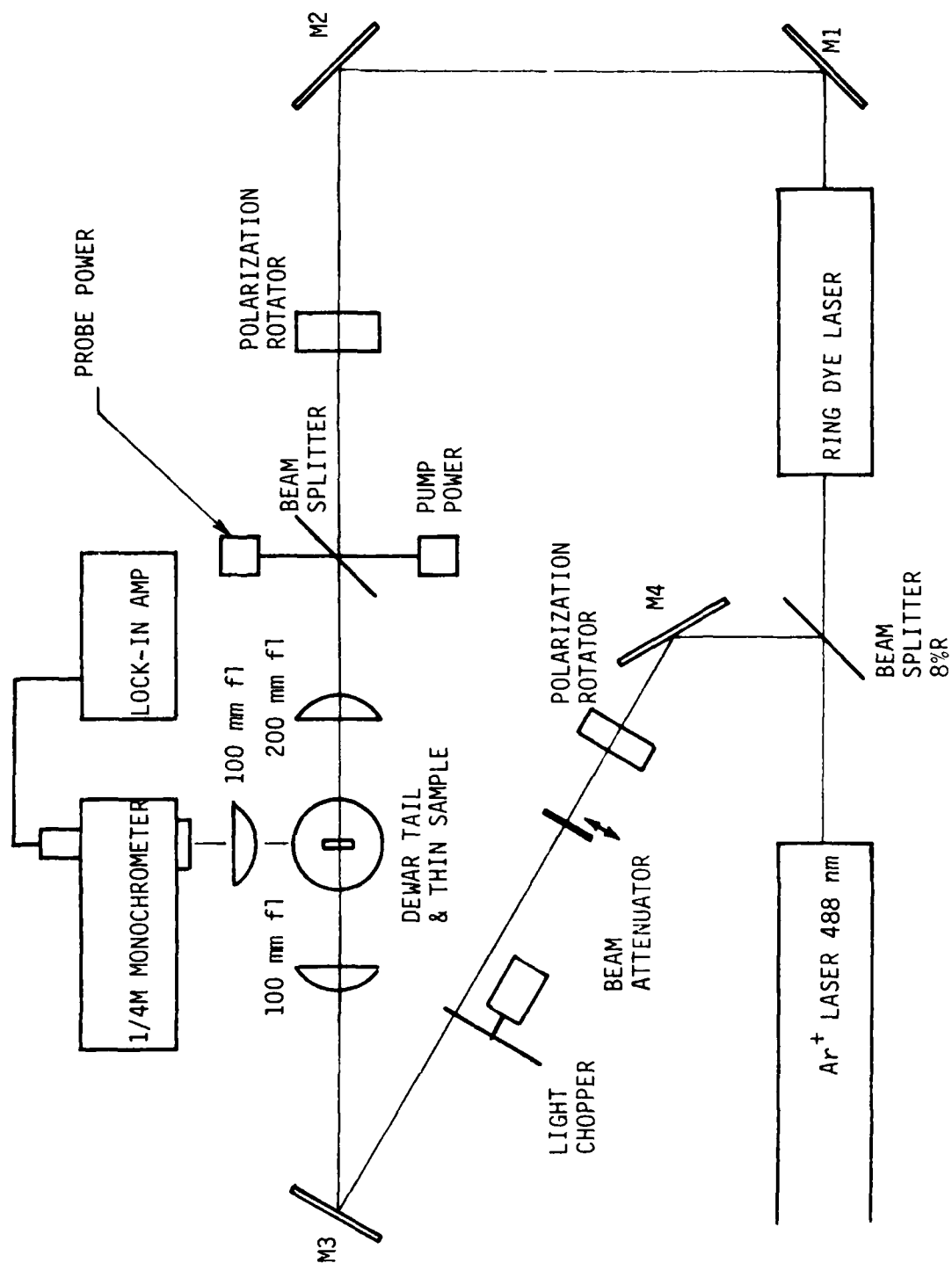Figure 2-5. Schematic Diagram of Modulated Population Experiment
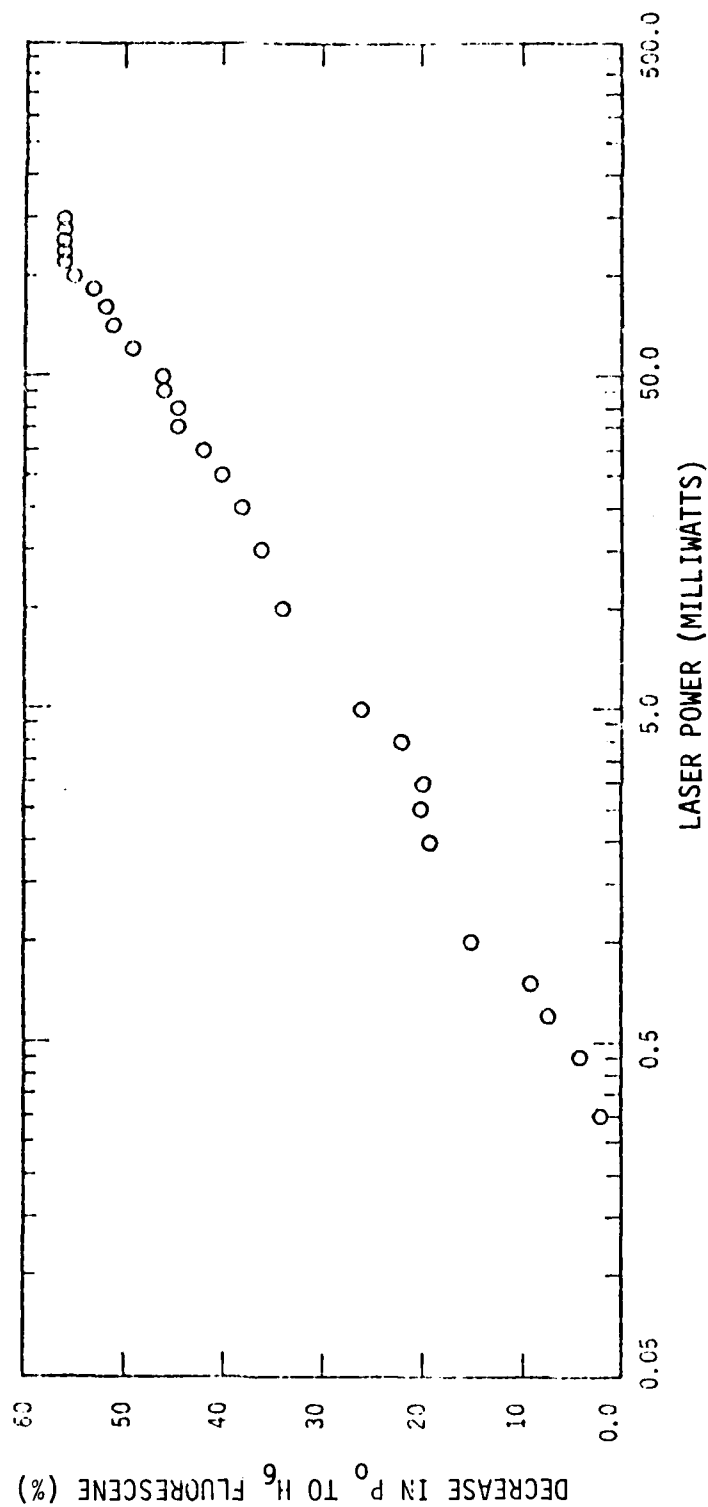
25

Figure 2-6. Ground State Population Change vs. Laser Pump Power - Ground State Population is Proportional to $P_0 - H_6$ Modulated Fluorescence
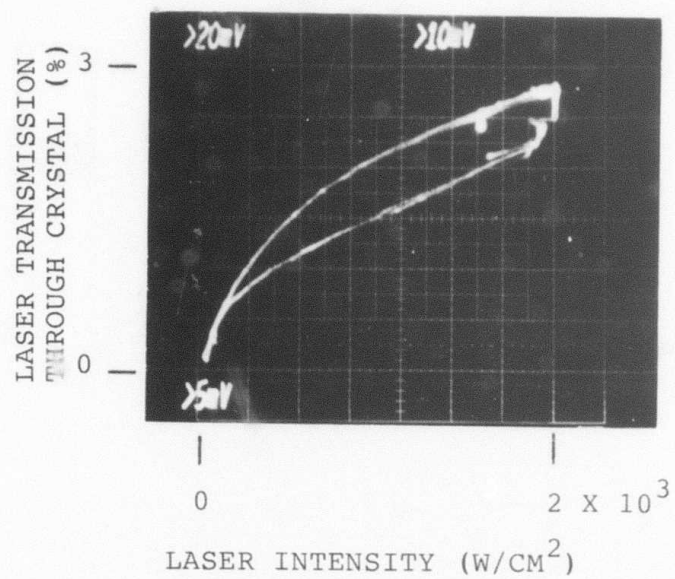
Figure 2-7. Avalanche Bistability

2.3 PRELIMINARY EVIDENCE FOR GAIN

A new dewar tail designed specifically for laser experiments was completed during the last period of the initial contract. This apparatus allowed for the mount of all intracavity surfaces at Brewster's angle. While the assembly was under construction, a few preliminary laser experiments were attempted. A 95 percent reflectivity mirror with 15 cm radius of curvature was aligned parallel to one face of the laser crystal. This face was then the other cavity mirror with approximately 15 percent reflectivity. An axial enhancement r^c 4-5 μm fluorescence was observed that can be attributed to the presence of laser action. Unfortunately, a conclusive interpretation was compromised by the observation that the enhanced signal was being coupled out of the cavity through the uncoated perimeter of the curved mirror. Since the cavity losses were large, the apparent laser action indicated a large gain coefficient of perhaps 1 or more per cm. A large gain should result in detectable beam characteristics and perhaps spectral line narrowing.

In order to test for gain a flat mirror ($\sim$100 percent R) was placed next to the face of the crystal. The experimental configuration is shown in Figure 2-8. The laser is focused with a cylindrical lens to a line at the entrance surface of the crystal. The mirror and exit surfaces were perpendicular to the gain filament thus formed. The gain filament was positioned normal to and opposed to the flat mirror and also above the mirror. These two positions, shown in the side view of the figure, correspond to 2ℓ and ℓ gain lengths, respectively. Here ℓ refers to the crystal thickness (4 mm). Two effects were observed. First, the output flux distribution from the crystal was much narrower with the mirror than without the mirror. A factor of four change in intensity was measured at 16.5 cm from the crystal. Second, the spectral content of the output was altered (Figure 2-10(c)). The strength of the $^3F_3 \rightarrow$ $^3H_4$ line to the ^3H-^3H bands was diminished by a factor of 4 from the ratio observed for a pont focus. These results strongly indicate gain in the 4-5 μm spectral region with an avalanche driven crystal.

2.4 LASER DEMONSTRATION

The avalanche laser was demonstrated conclusively during the final month of the previous contract. The new dewar tail was incorporated into the experiment
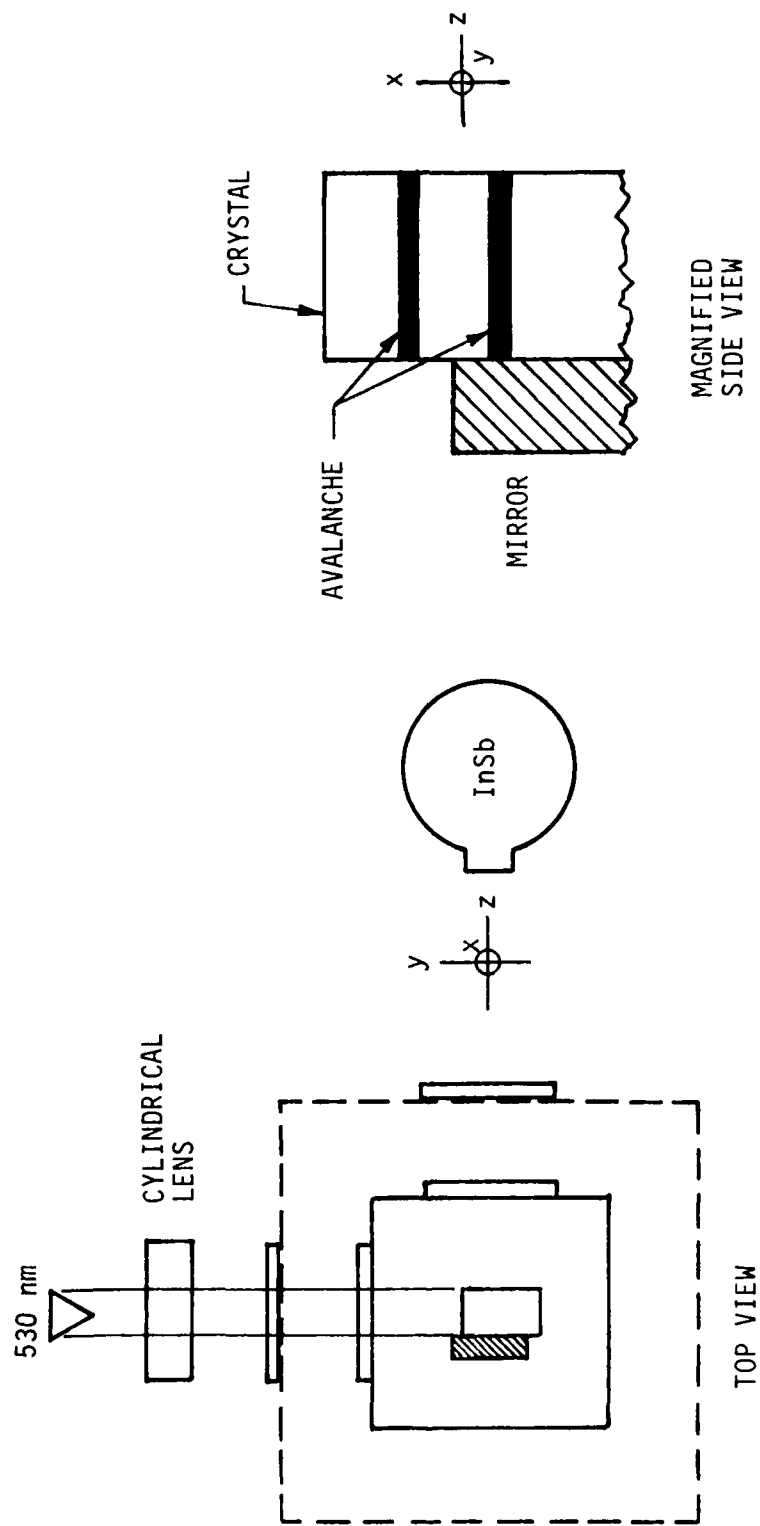
Figure 2-8. Schematic Diagram for Initial Laser Experiments

allowing for the inclusion of Brewster surfaces in the cavity. The experimental arrangement is shown in Figure 2-9. Two cylindrical lenses were used to focus the pump laser to a linear filament on the side of the crystal. M2 was a 190 mm radius, ~100 percent R, aluminized mirror held at 190 mm from the flat mirror. The flat mirror was designed and coated at the ATC thin film laboratory and had a 95 percent reflectivity from 4 to 5 μm. The crystal was shaped so that π line emission, normal to the mirrors, would exit the crystal at Brewster's angle (π configuration). The cavity parameters for the demonstration are listed in Table 2-1.

TABLE 2-1 CAVITY PARAMETERS FOR FIRST AVALANCHE LASER

o 3.82 Molar Percent Pr in $LaCl_3$ Host
o 125K
o Transverse Excitation (100 mW & 529.2 nm)
o π Line Configuration
o 1.98 mm Gain Length
o 190 mm Cavity Length
o $\cong$100% R / 190 mm Radius + 95% R / Flat
o 110 μm Pump Focal Volume Diameter

The cavity spectral output is shown in Figure 2-10a). As in the spectrum from the gain filament (same Figure), the $^3F_2$ - $^3H_4$ emission is relatively small. Note, however, the appearance of a new feature at 4.8 μm. The laser output was concentrated in a beam. A 4.5 mm diameter (FWHM) spot at a distance of 320 mm from the crystal was typical. This beam disappeared when the back mirror was blocked. Specifically, the intensity dropped by a factor of up to 80, when suitably apertured. The power output was determined after calibration of the InSb detector to be 5 μW. The various output parameters are listed in Table 2-2.

(A) TOP VIEW

(B) SIDE VIEW

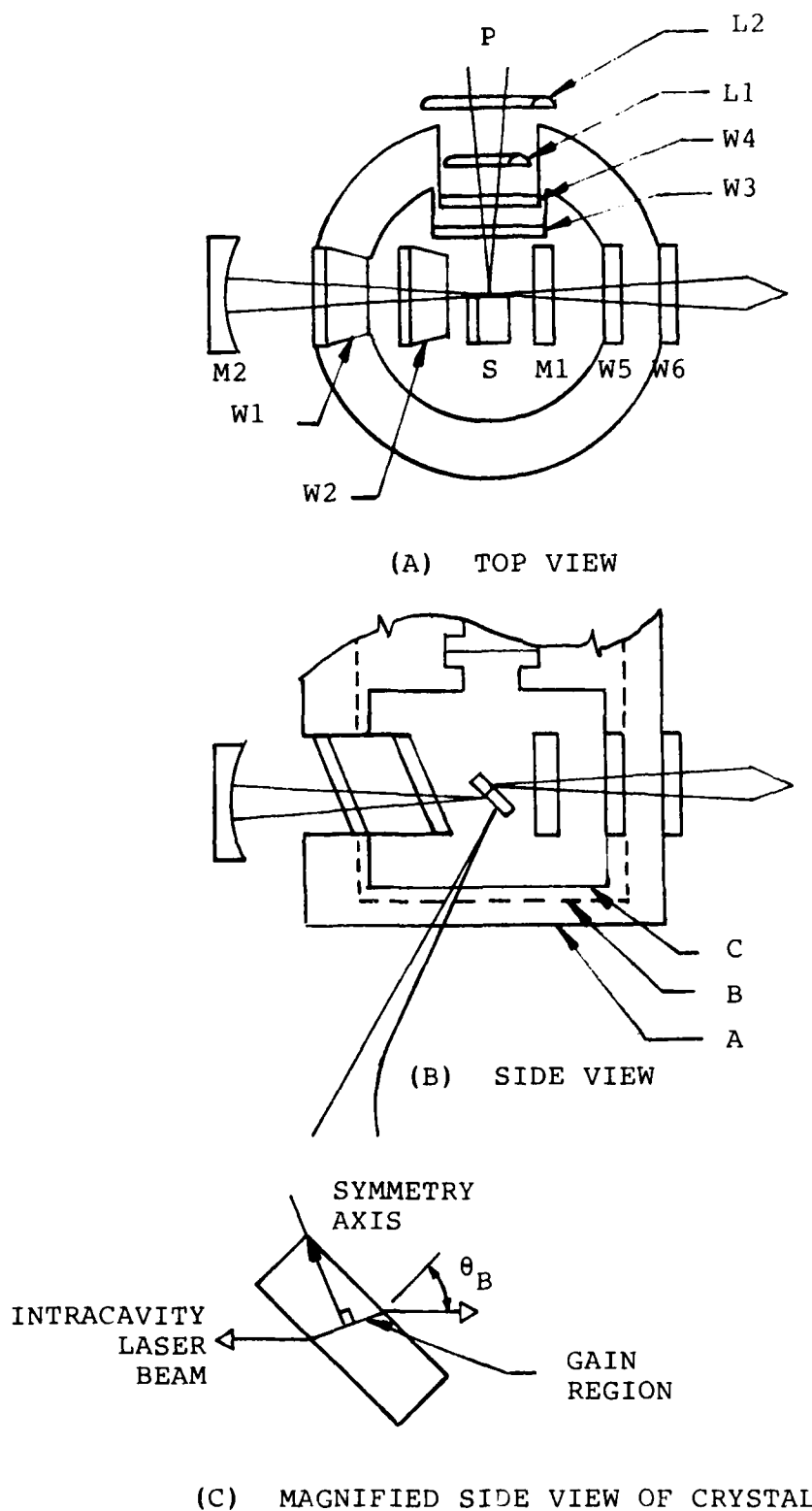(C) MAGNIFIED SIDE VIEW OF CRYSTAL

Figure 2-9. Schematic Diagram of First Photon Avalanche Laser
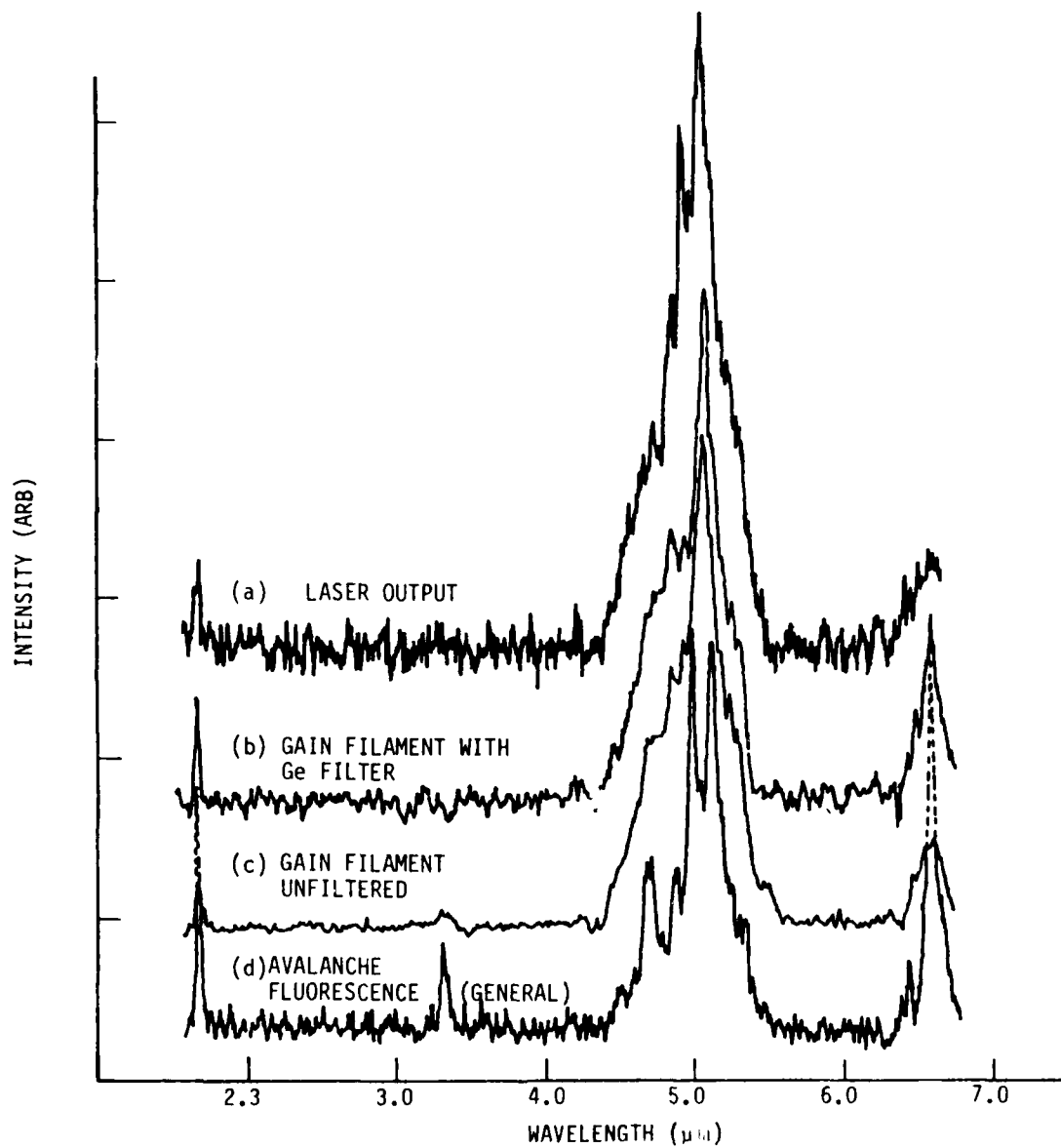
Figure 2-10.   Avalanche Fluorescence From Various Experiments

32

TABLE 2-2 OUTPUT CHARACTERISTICS FOR FIRST AVALANCHE LASER

PARAMETER	VALUE	UNITS
POWER	5	μW
WAVELENGTH	4.9	μm
BEAM DIVERGENCE	14	mR
SPOT DIVERGENCE	4.5	mm @ 320 mm
WALL PLUG EFFICIENCY	2×10^{-8}	%
LIGHT EFFICIENCY	3×10^{-3}	%

Laser beam shape was examined in detail in the far field. As shown in Figure 2-11 the output beam exhibited an oval cross-section. Assuming a diffraction limited beam, the observed divergence implies an asymmetric cross-section for the cavity mode with dimensions of approximately 665 μm vertically and 250 μm horizontally. The vertical extent of the focused pump laser beam was measured at approximately 120 μm. Thus, cavity mode size greatly exceeds the gain region, at least for the vertical dimension. The mismatch leads to high diffraction losses and acts to reduce available output power. Also, high loss implies a large gain coefficient, consistent with earlier experiments.

NARROW BEAM

    o DIMENSIONS IN MM

    o ΔX or $\Delta Y = e^{-2}$ OF INTENSITY

CRYSTAL

GAIN VOLUME

y

z   x

Z = 420
ΔX = 9.7
ΔY = 3.9

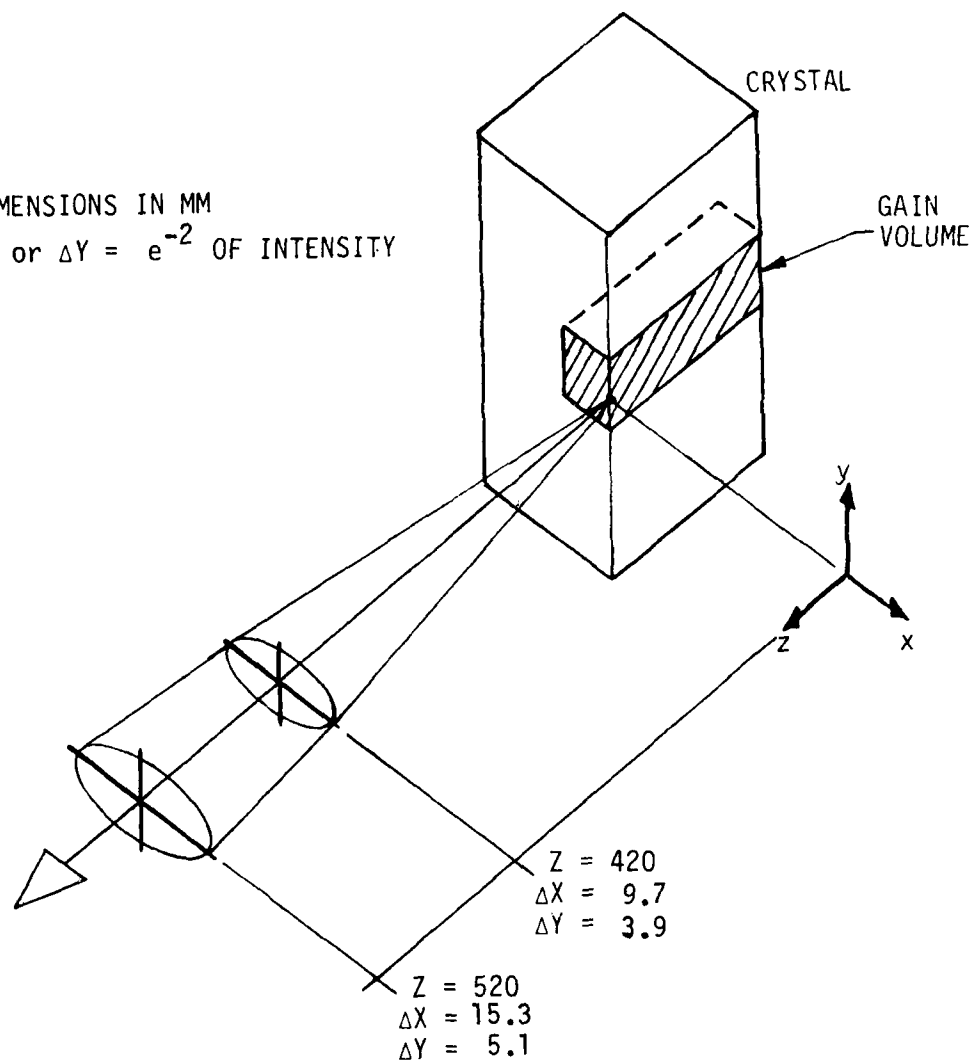Z = 520
ΔX = 15.3
ΔY = 5.1

Figure 2-11. Far-Field Beam Profile of Avalanche Laser

3.0 TECHNICAL RESULTS

3.1 CRYSTAL GROWTH

Crystal processing, throughout the extent of this contract, presented technical challenges which severely effected the outcome of various experiments. In each case, as problems arose, solutions were found. Yields and optical quality were improved immensely and a new technique for removing a major impurity, LaOCl, was developed.

The first five attempts at crystal growth ended with shattered growth ampoules, occuring during the warm-up phase in the Bridgeman process. The problem was traced to a new cleaning procedure employed by the quartz-ware vendor, specifically an HF cleaning step had been added prior to distillation cell fabrication. This resulted in very clean and probably pebbled surfaces causing enhanced wetting of the quartz by the molten rare earth salt. Subsequently, problem developed in the crystal growing phase since, at that point, the standard procedure requires a multiple melt-freeze sequence in the growth ampoule, not encountered in previous processing steps. The wetting of the HF etched quartz by the molten salt after two such cycles was sufficient to cause breakage of the ampoule upon reheating due to the difference in thermal expansion between $LaCl_3$ and SiO_2. The breakage problem vanished when the HF cleaning step was discontinued.

The resolution of the ampoule breakage problem was delayed by the long cycle time from the beginning of the materials preparation process to grown crystal. Historically, very low yields have been achieved in our laboratory. The crystals are generally cracked throughout with only one in four yielding usable sections of crystal. Because of these low yields and and the lost time due to the breakage problem an attempt was made to improve the processing by adjusting the temperature gradient during the cooldown phase of the Bridgeman process. This was a logical step based on considerations elaborated upon in the literature on the subject.[6] The symptom of cracked crystals, ie., polycrystallinity, was assumed as evidence for too large a cooldown gradient. Efforts to lower the gradient were thwarted by a brass cylinder inserted in the oven by previous investigators. A cutaway view of the oven is shown in Figure 3-1.
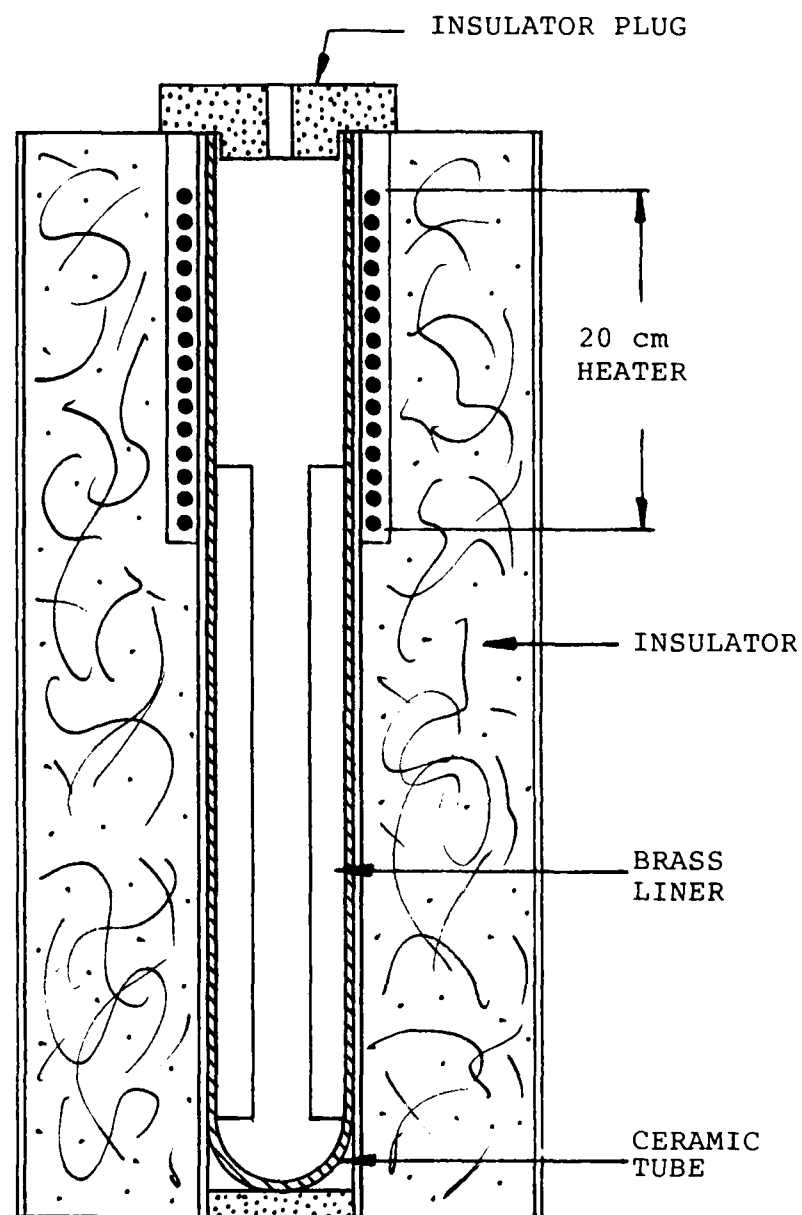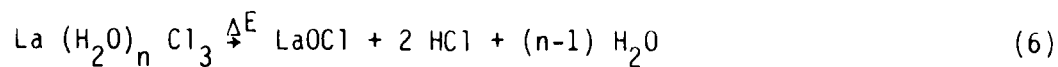
Figure 3-1. Crosssection of Marshall
Furnace Modified for Bridgeman
Growth

36

The purpose of the brass liner was to increase the thermal gradient. When this liner was removed, the desired gradient (20C above to 50C below the melting point in 5cm) was more nearly approached. Both the original and final thermal profiles are shown in Figure 3-2.

The results of the change in thermal profile were astonishing. The next four attempts yielded one crystal with a single crack, which upon examination later in the contract was found to be impregnated with bubbles, and three large and high optical quality crystals. Production yields had thus increased enormously.

All of the above events, except the last crystal growth, took place before the time consuming move to the new laboratory in May. Large crystals were available for experimentation at three desirable dopant levels, including the first photon avalanche laser dopant level and significantly higher and lower levels. Consequently, the move was not seen as strongly effecting the experimental results. After the move, however, direct attempts at laser action with new materials were impeded when the bubble problem was discovered in the crystal with the dopant level (3.96%) nearest the original laser crystal level (3.82%). In addition, the move was accompanied by various facilities, laser and vacuum problems. The final crystal was grown in the new laboratory facility and was largely a high optical quality single crystal but with a lower than desired dopant level. Experiments were thus confined to two new crystals with 2.75 and 5.2% dopant levels and the small amount of the original crystal left. A summary of the growth history of the crystals and the inventory left from previous work is given in Table 3-1.

The final crystal grown did not yield a dopant level closer to that of the original laser crystal than crystals already available. The target level was precisely that of the original laser crystal. We believe that this lack of accuracy in controlling dopant levels is directly attributable to the presence of large impurity levels in the base stocks. The impurity, LaOCl, is a byproduct of $La(H_2O)Cl_3$ and modest ΔE.[6]

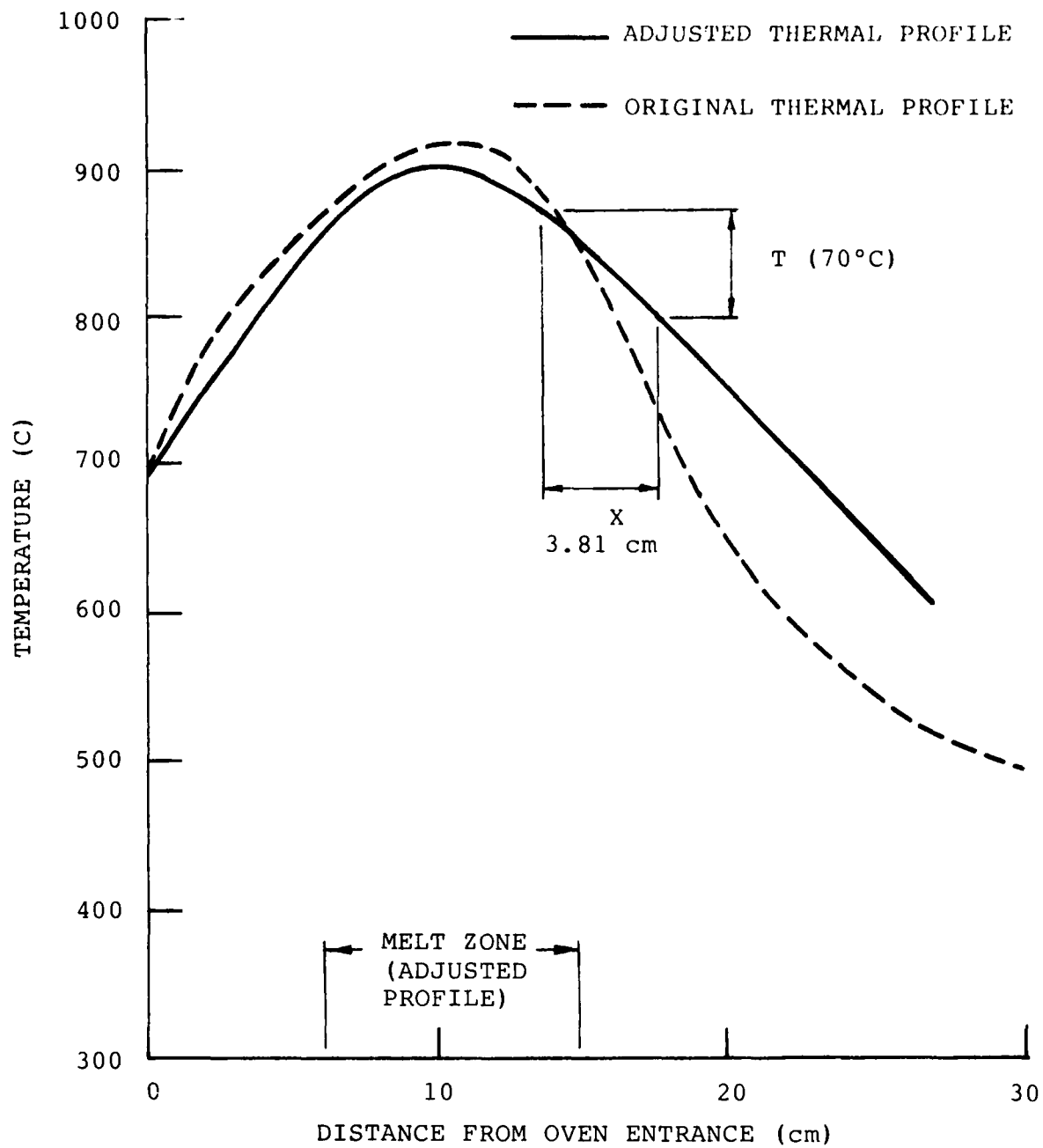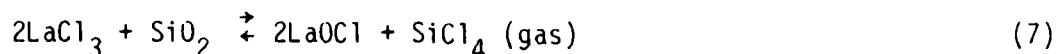$$La\,(H_2O)_n\,Cl_3 \overset{\Delta E}{\rightleftharpoons} LaOCl + 2\,HCl + (n-1)\,H_2O \tag{6}$$

Figure 3-2. Marshall Furnace Thermal Profiles

The reaction takes place during the vacuum bake cycle intended to remove H_2O. The level of this contamination can be measured by dissolving a small amount of crystal in H_2O. A white residue precipitates. This residue can be washed with flowing water, filtered, dried, and weighed. The level of contamination of our crystals was found to be as high as 2.5% LaOCl by weight. Both the zone refining and distillation steps are designed to remove the LaOCl which is both solvable in molten $LaCl_3$ and relatively refractory. Unfortunately, the molten $LaCl_3$ reacts with the quartz distillation cell forming new LaOCl in, perhaps, higher quantities. This new reaction,[7]

$$2LaCl_3 + SiO_2 \rightleftarrows 2LaOCl + SiCl_4 \text{ (gas)} \tag{7}$$

would reach equilibrium in a sealed cell thus limiting production of LaOCl. However, our distillation process is carried out while actively pumping on the material. This reduces the partial pressure of the $SiCl_4$ and correspondingly increases the production of LaOCl. The wetting of the quartz vessel by the molten rare earth salt is probably enhanced in part by this reaction. In summary, we feel that $LaCl_3$ crystals produced by methods employing a quartz distillation step are seriously contaminated with LaOCl.

A new crystal production process is being implimented in our laboratory. The process will employ niobium lined SiO_2 vessels. Zone refining will be temporarily discontinued. The first step in the process will be multiple distillation carried on until LaOCl residue is minimized. The salts will then be mixed in the desired proportion and a crystal grown. High yield, quality, and purity levels are anticipated in crystals grown to support future efforts.

TABLE 3-1. CRYSTAL STOCKS

CRYSTAL	MOL % Pr	DATE GROWN	COMMENTS	OLD ΔT	NEW Δ^T
6-76	2.01	Earlier Work	-	✓	
A-33	3.82	Previous Contract	Original Laser	✓	
A-35	5.12	"	-	✓	
4-140	7.38	"	-	✓	
A-52	5.8	"	-	✓	
B-3	-	12-12-83	Broken	✓	
B-4	-	1-10-84	Broken	✓	
B-5	-	1-12-84	Broken	✓	
B-11	-	2-2-84	Broken	✓	
B-13	-	2-6-84	Broken		
B-14	5.2	2-3-84	Largely Usable	✓	
B-20	-	3-2-84	Broken	✓	
B-21	3.96	3-7-84	Bubbles		✓
B-23	2.2	3-27-84	Largely Usable	✓	✓
B-30	2.66	4-25-84	Largely Usable	✓	✓
B-45	2.75	9-17-84	Large Lower Section-Hi Quality		✓
		9-17-84	Small Upper Section Bubbles		✓

3.2 CAVITY DESIGN

3.2.1 Physical Constraints

The design of the laser cavity was governed in part by physical con-
straints imposed by apparatus built for the first photon avalanche laser and a
need to keep modifications to a minimum. Additionally, two key criteria were
identified during work under the previous contract, namely, a need to change
the laser focus over a large range of values and the practical necessity for
output coupler mirror changes without breaking the vacuum integrity of the
system. Because of the above design requirements, a three element cavity

composed of two flat mirrors with an intermediate positive lens was chosen. A schematic diagram showing key elements of the design in relation to the original experimental cell is shown in Figure 3-3. The output coupler flat mirror (M1) is located outside of the dewar tail while the lens (L) position is adjustable between as near to the sample (S) as possible (1) and a position (2) near the inverted Brewster window mounting (B). A second flat mirror (M2) is positioned as close to the crystal as possible, as in previous experiments.

3.2.2 Final Design

The final design allowed for transverse as well as axial pumping experiments. A cutaway drawing of the laser is shown in Figure 3-4. The pump laser beam can enter from one of two directions (1 or 2) depending upon whether the laser is respectively pumped transversly or longitudinally. The crystal, S, is held in place in a sample cell (dashed lines) needed for transfer from a dry box to the dewar. A flat mirror M2 is held in place by an assembly (MM2) sealed in the sample chamber but connected to the outside of the dewar tail by three rotatable rods. These rods allow for mirror positioning adjustments but can be disconnected from the sample cell by pull-apart couplings located between the sample chamber and the dewar tail walls. Thus, thermal leaks are minimized during the experiment. M2 is either a dichroic (axial pump) or a simple gold coated high reflector (transverse pump) mirror. The intracavity lens (L) is sealed to the end of a tube which can be screwed in and out along the laser axis. The other flat mirror, M1 (output coupler), is also mounted on the end of a cylinder which is in turn attached to an angular orientation device fixed to the experimental table. More details of the laser assembly are shown in Figure 3-5.

3.2.3 Cavity Stability and Spot Sizes

The cavity shown in Figure 3-3 is stable under a variety of conditions. These conditions can be determined by examining the unit matrix for this cavity.
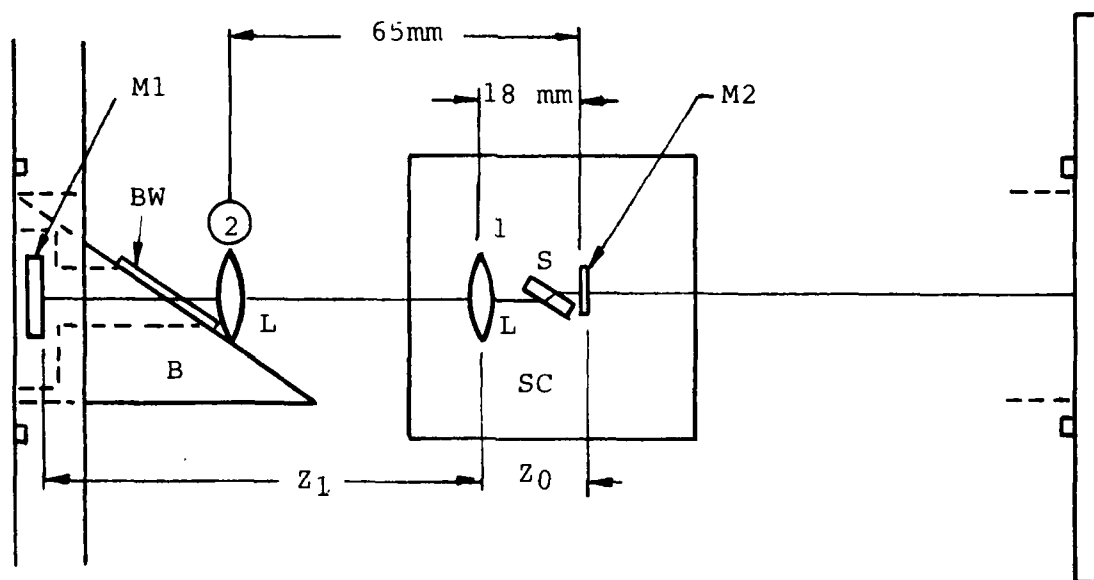
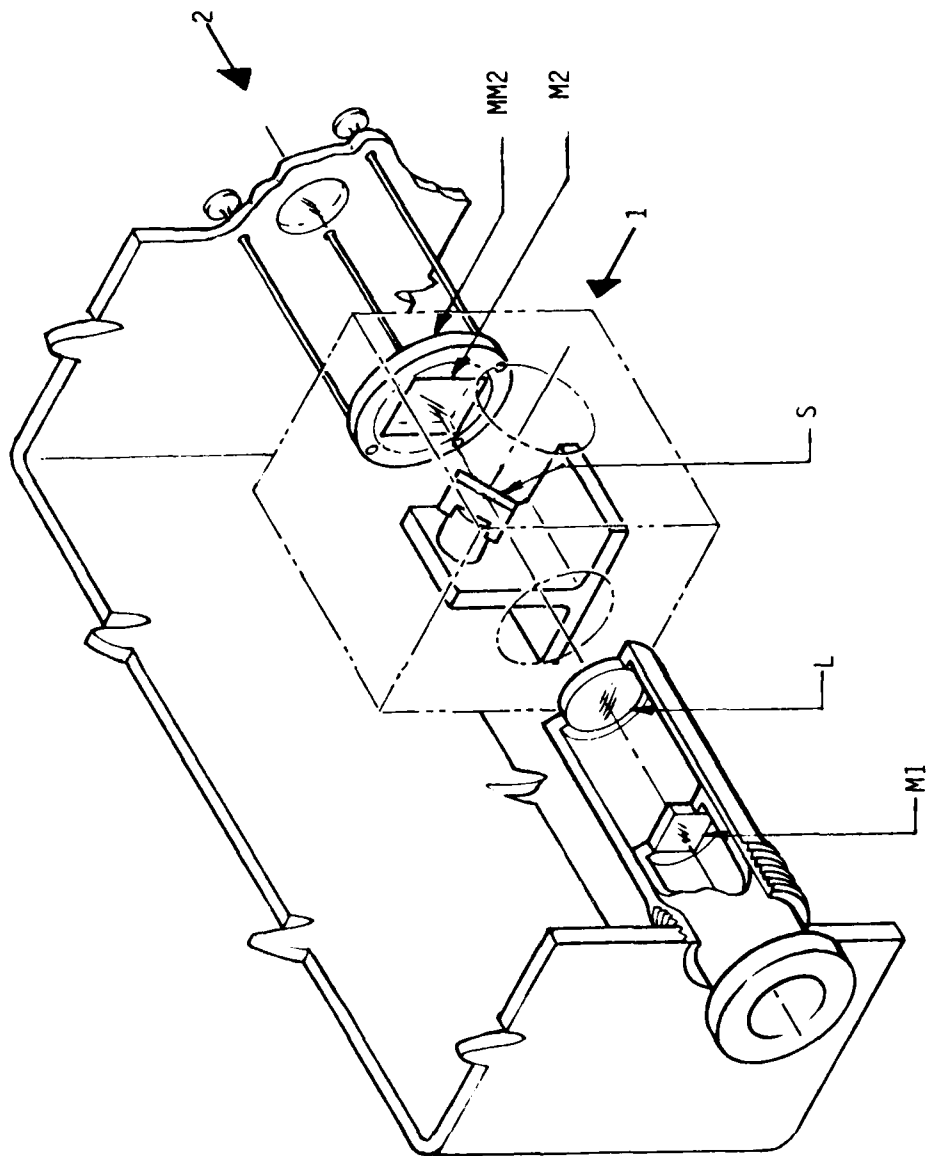Figure 3-3. Constraints on Lens Position Imposed by Existing Apparatus

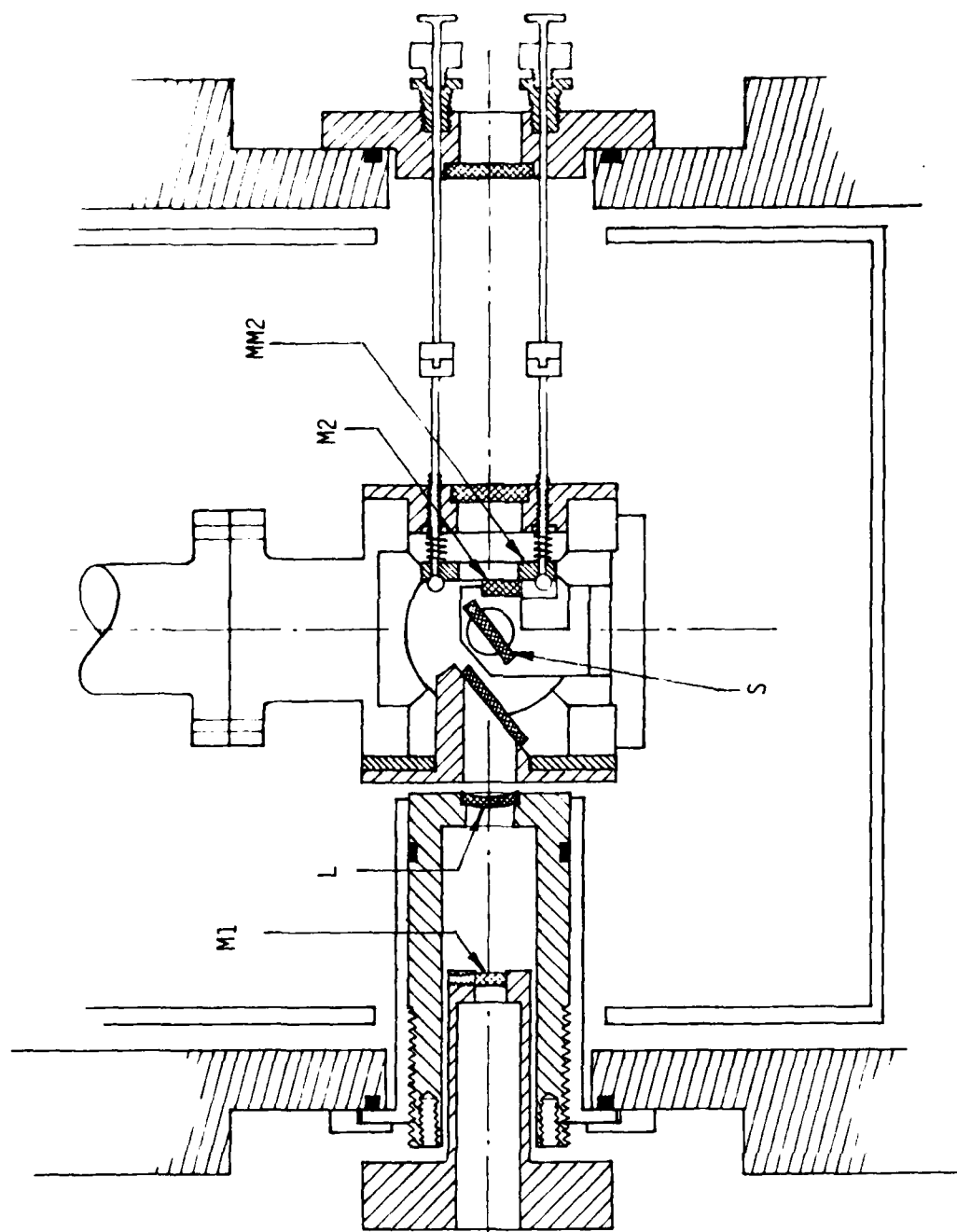Figure 3-4. Cutaway View of Photon Avalanche Laser Apparatus

Figure 3-5. Crossection of Photon Avalanche Laser Apparatus

44

$$\begin{bmatrix} A & B \\ C & D \end{bmatrix} = \begin{bmatrix} 1 - \dfrac{z_1}{f} & z_0 + z_1(1 - \dfrac{z_0}{f}) \\ -\dfrac{1}{f} & 1 - \dfrac{z_0}{f} \end{bmatrix} \qquad (8)$$

The stability criterion is $-1 < (A+D)/2 < 1$ which from Equation (8) leads to $0 < (1-z_0/f)(1-z_1/f)-1$. The formal similarity between this result and that for two mirror cavities is evident. The regions of stability are shown in Figure 3-6. The lens focal length was chosen by demanding a range of spot size at M2 (near the crystal) from 50 to 500 μu within the lens position adjustment allowed by the apparatus. The spot sizes at M1 (ω_0), L (ω_2), and M2 (ω_1) are shown in Figure 3-7 for a focal length of 38 mm and a cavity length of 100 mm (minimal length easily achieved). These spot sizes are calculated at a position within the cavity by demanding that the Gaussian beam transform into itself after one cavity round trip:

$$w_0^{\,2} = \frac{\lambda f}{\pi} \left[(1 - \frac{z_0}{f})(\frac{z_1}{f - z_1} + \frac{z_0}{f}) \right]^{1/2}$$

$$w_1^{\,2} = \frac{\lambda f}{\pi} \left[(1 - \frac{z_1}{f})(\frac{z_0}{f - z_0} + \frac{z_1}{f}) \right]^{1/2}$$

$$w_2^{\,2} = w_0^{\,2} \left[1 + (\frac{\lambda z_0}{\pi w_0^{\,2}})^2 \right]$$

Stability of this cavity for a total length 100 mm and various focal lengths is further explored in Figure 3-8.

3.2.4 Lens and Coating Design

Spot diagrams indicating achievable spot sizes, sensitivity of a focal spot to angular misallignment as well as a ray trace diagram, and the lens
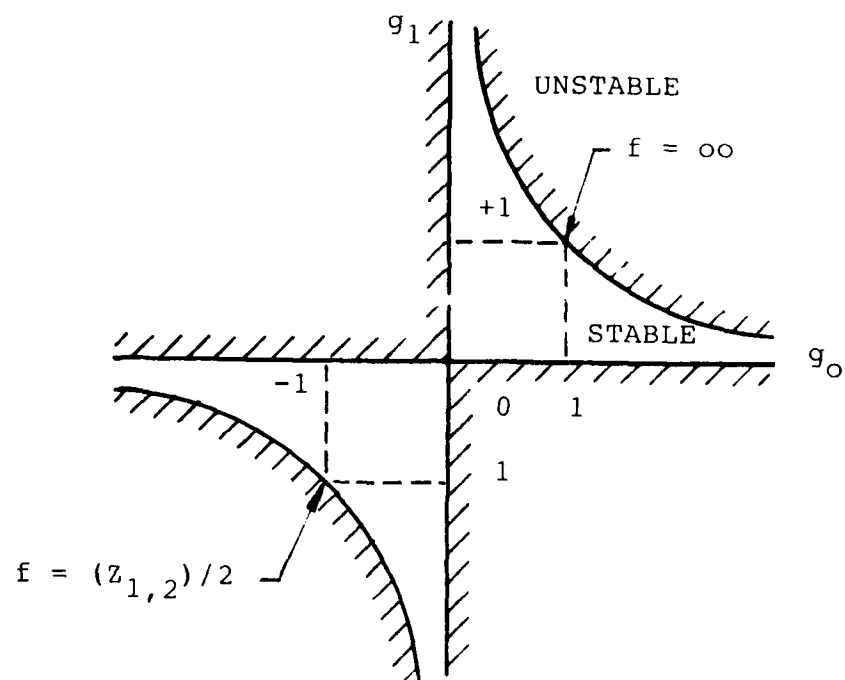
45

Figure 3-6.   Stability of 3 Element Cavity,
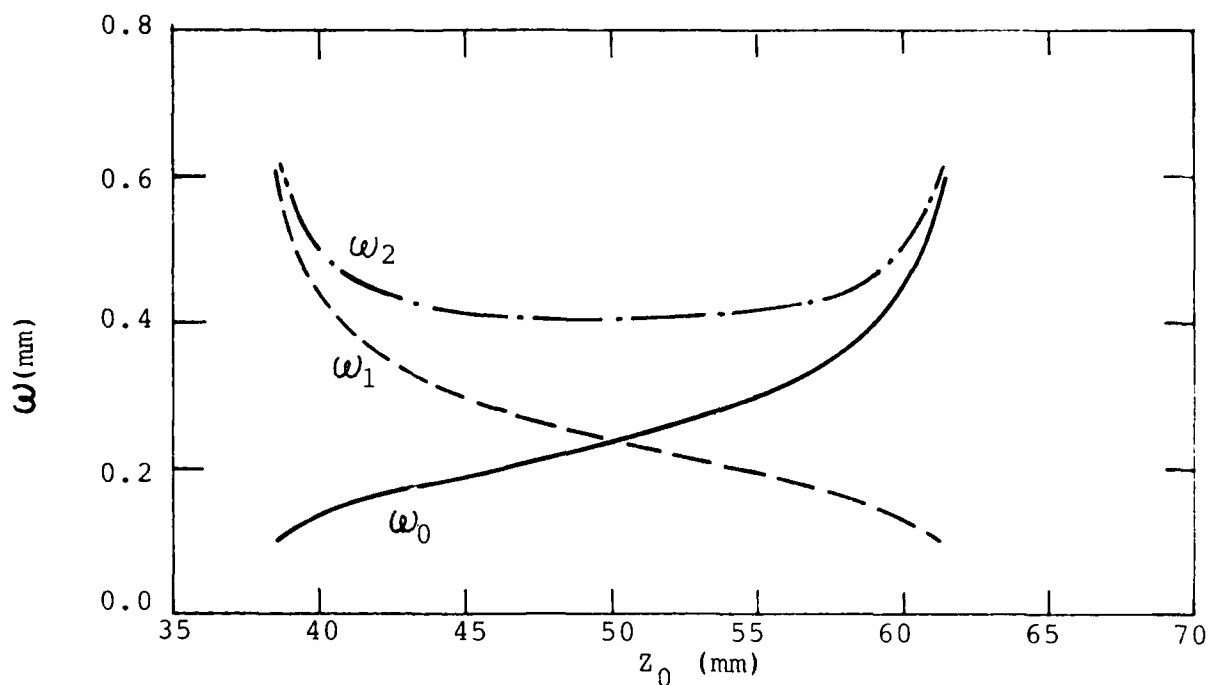$g_0 = 1 - Z_0/f$, $g_1 = 1 - Z_1/f$

Figure 3-7. Intra Cavity Spot Sizes
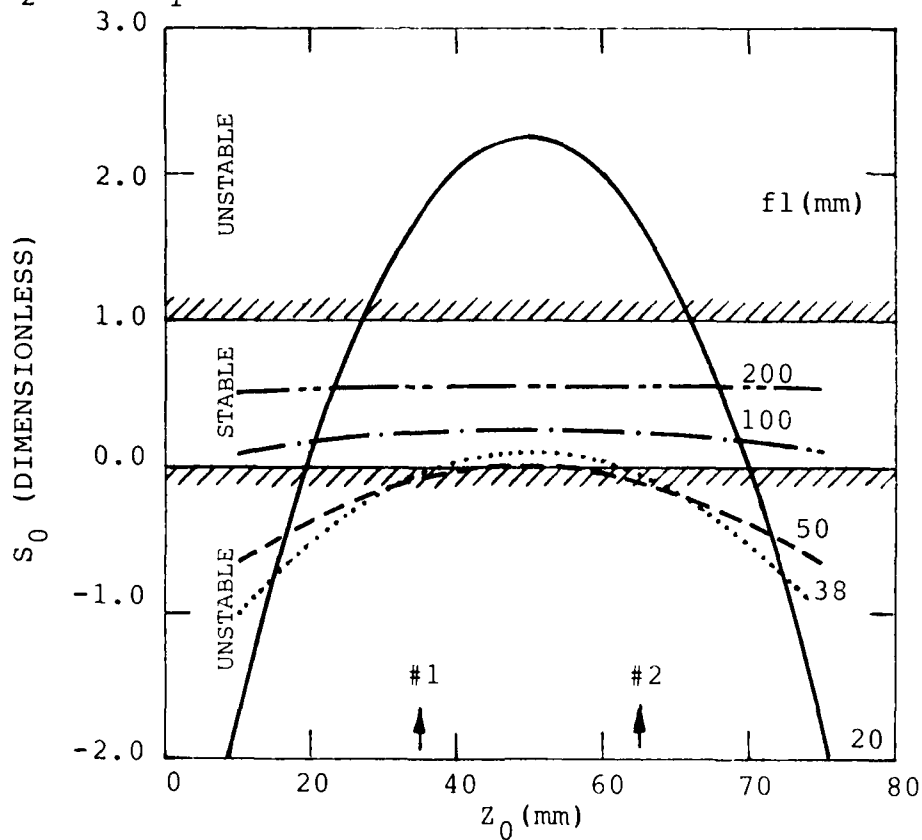ω_0(M2), ω_2(L), ω_1(M1), Cavity Length = 100 mm, f = 38 mm

Figure 3-8. Stability Factor $S_0 = (1 - Z_0/F)(1-Z_1/f)$
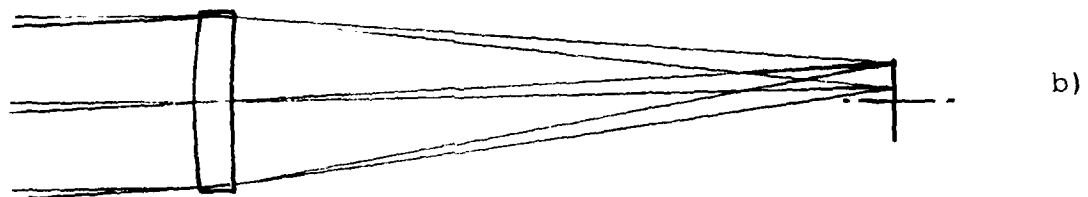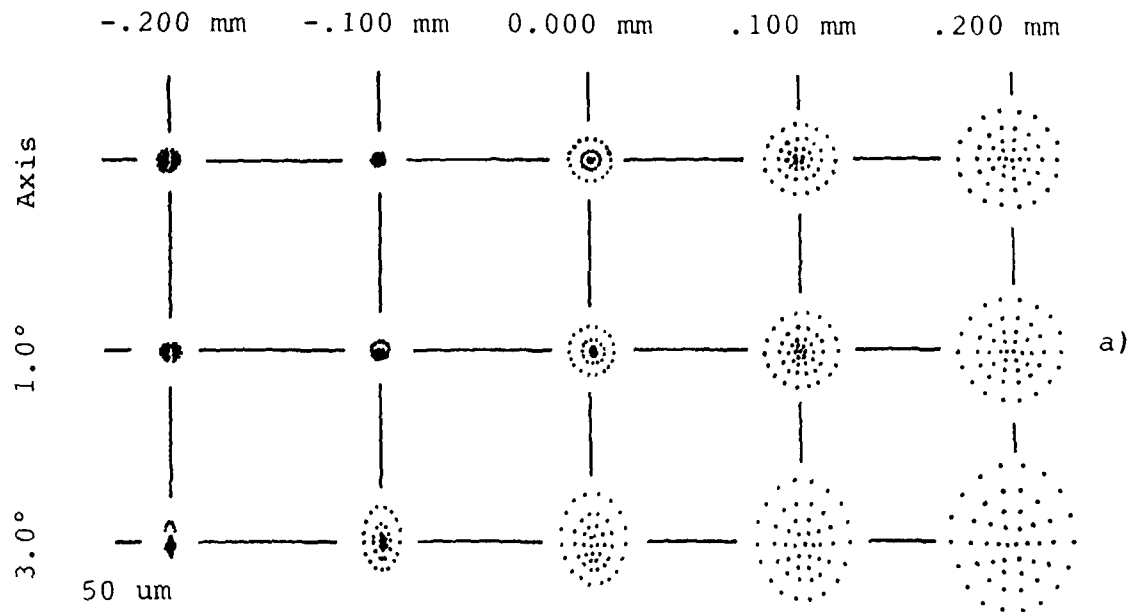for f = 38 mm, Cavity Length = 100 mm

47

design parameters are shown in Figures 3-9a), b), and c) respectively. The
lens was made from ZnSe and AR coated on both sides. The performance of this
coating is shown in Figure 3-10 along with the performance of various coating
and substrate combinations used for output coupler mirrors. Dichroic mirrors
were fabricated by CVI corporation in Albuquerque. The performance of these
mirrors was marginal with a very good IR high reflector but low transmission at
the pump wavelength (30%). The infrared reflectance of a CVI mirror is shown
in Figure 3-11.

3.3 LASER PERFORMANCE

3.3.1 Preliminary Laser Performance

Prior to the completion of the intercavity lens assembly, an attempt was
made to reestablish laser action with the original photon avalanche laser crys-
tal. The apparatus was the same as used in the initial demonstration except
for the addition of the flat mirror adjustment assembly, MM2 shown in Figure
3-5. The experimental objectives were threefold: first, to validate the design
of the mirror adjustment assembly by operational testing; second, to determine
if the degradation in laser output observed during PAL1 was due to deteriora-
tion of the crystal quality or to experimental problems not related to the bulk
properties such as surface contamination or finish, vacuum leaks, etc. third,
to compare the temporal properties of laser output with bulk avalanche fluores-
ence.

The laser showed further deterioration in spite of improved alignment with
the adjustment capability of MM2 as well as the extreme attention placed on-
surface polish and alignment. A performance characteristic, the ratio of on
axis intensity with a complete cavity to the intensity with a blocked curved
mirror, decreased from seven in the first setup to five in the second to three
in the third and then approximately two in the final (this contract) experi-
ment. The latter value was expected even without gain if retroreflected light
from the curved mirror was directed to just miss the crystal on the way to the
detector. These results are both consistent with degradation of the bulk crys-
tal, perhaps due to thermal cycling followed by incipient cracking, or from
loss of gain length, perhaps due to the polishing step prior to each operation.
The modulated population experiments conducted during the first program also

48

-.200 mm   -.100 mm   0.000 mm   .100 mm   .200 mm

Axis

1.0°

3.0°

50 um

FOCAL LENGTH = 38.100 mm.   ALL DATA IN mm

RADIUS	SEPN	CL.DIAM	MATERIAL
34.519		9.91	
	2.000		2.41860
92.288		9.91	
	36.805		Air
IMAGE PLANE		4.77	

Figure 3-9.   Intercavity Lens Performance
            a)   Spot Diagrams, b) Ray Trace,
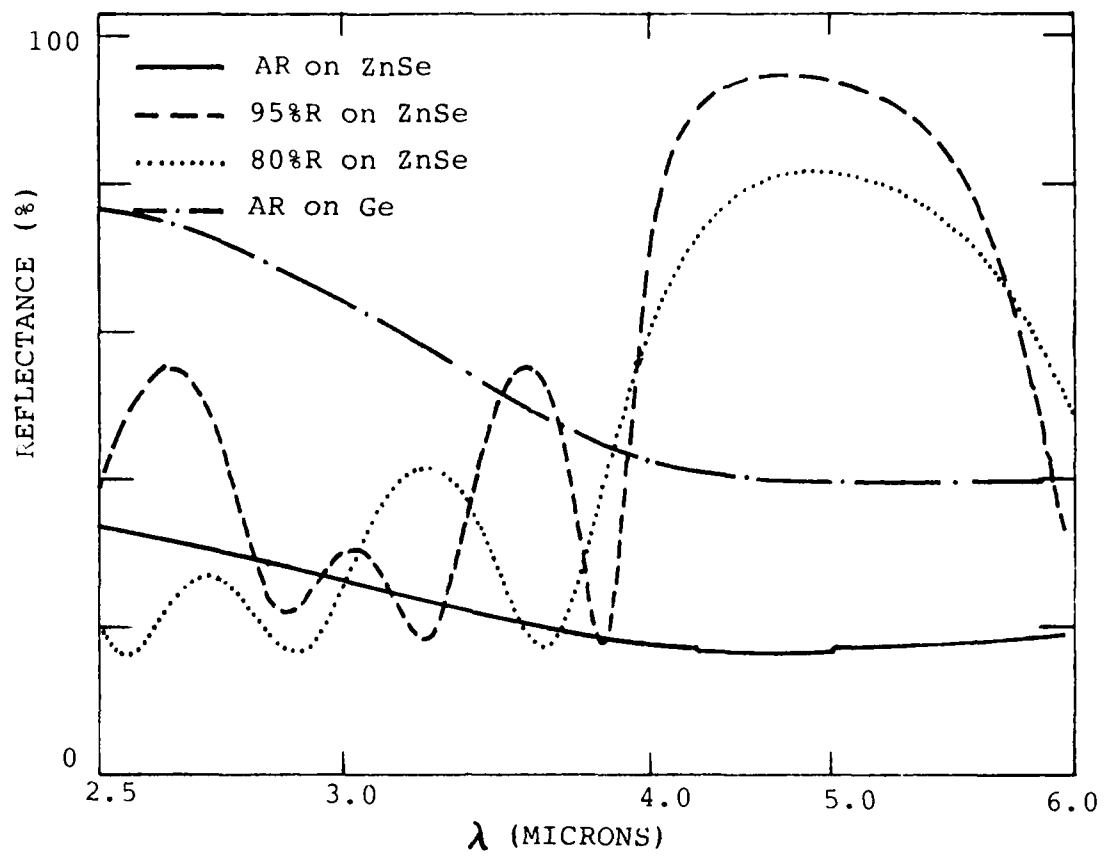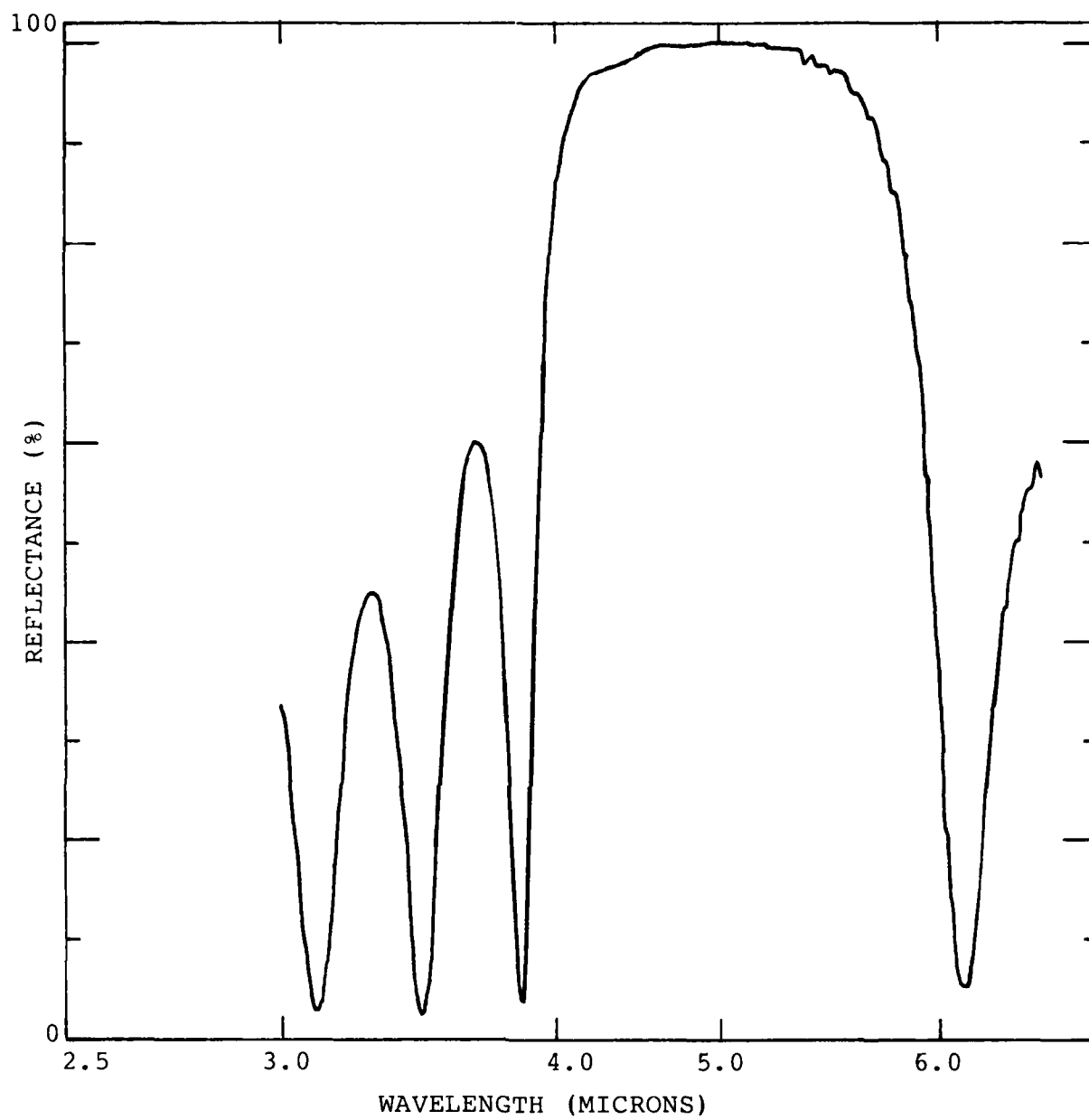   c)   Lens Parameters

Figure 3-10. Coating Performance

Figure 3-11. Infrared Reflectance of CV1 Dichroic Mirror

51

also showed an apparent degradation of performance. That is arly results indicated an inversion of the $^3P_0$ over the $^3H_4$ state populations. The ground state population was found to be depleted by up to 70% but this number later fell to slightly above 50%. Planned experiments were expected to overcome all previous experimental problems. Due to failure of the laser to operate, the temporal experiments were delayed until an operating laser was available.

3.3.2 Modulated Population Experiment

The modulated population technique described in an earlier section was implemented under the present contract for only a short while. During that time the response of one of the crystals (B14) grown during this program was tested. The experiment was altered slightly from that conducted during the first contract by the addition of a two prism wavelength selection scheme as shown in Figure 3-12. This allows for operation of all lines from the Ar^+ laser and selection of probe wavelengths other than 488.0 nm; however, only the ground state population probe (488.0 nm) was used. The sample tested showed the ground state population decreasing to 68% of the value at 100°K. Although quite large compared with the difference in population necessary for most conventional lasers, it is significantly lower than depopulation levels measured previously (see previous paragraph). This experiment was not operational until the last quarter when laser performance improvements became paramount. Therefore the question as to whether the low depopulation level was due to individual crystal properties, or external parameters, was not answered.

3.3.3 Avalanche Hysteresis

The hysteresis loop discovered under the previous contract was further investigated. The experimental setup remainded the same but with more time devoted to sorting out problem areas. Nonlinear detector response was minimized by careful selection of filters. The origional loop was found to be a composite of a crystal hysteresis loop and bistability in a 530 nm line filter placed in front of the transmission detector. The final hysteresis loop obtained is shown in Figure 3-13. This loop does not exhibit the permanence of the original composite loop. If taken slowly enough, over a period of approximately 15 minutes, no loop is observed. This is consistent with an expected
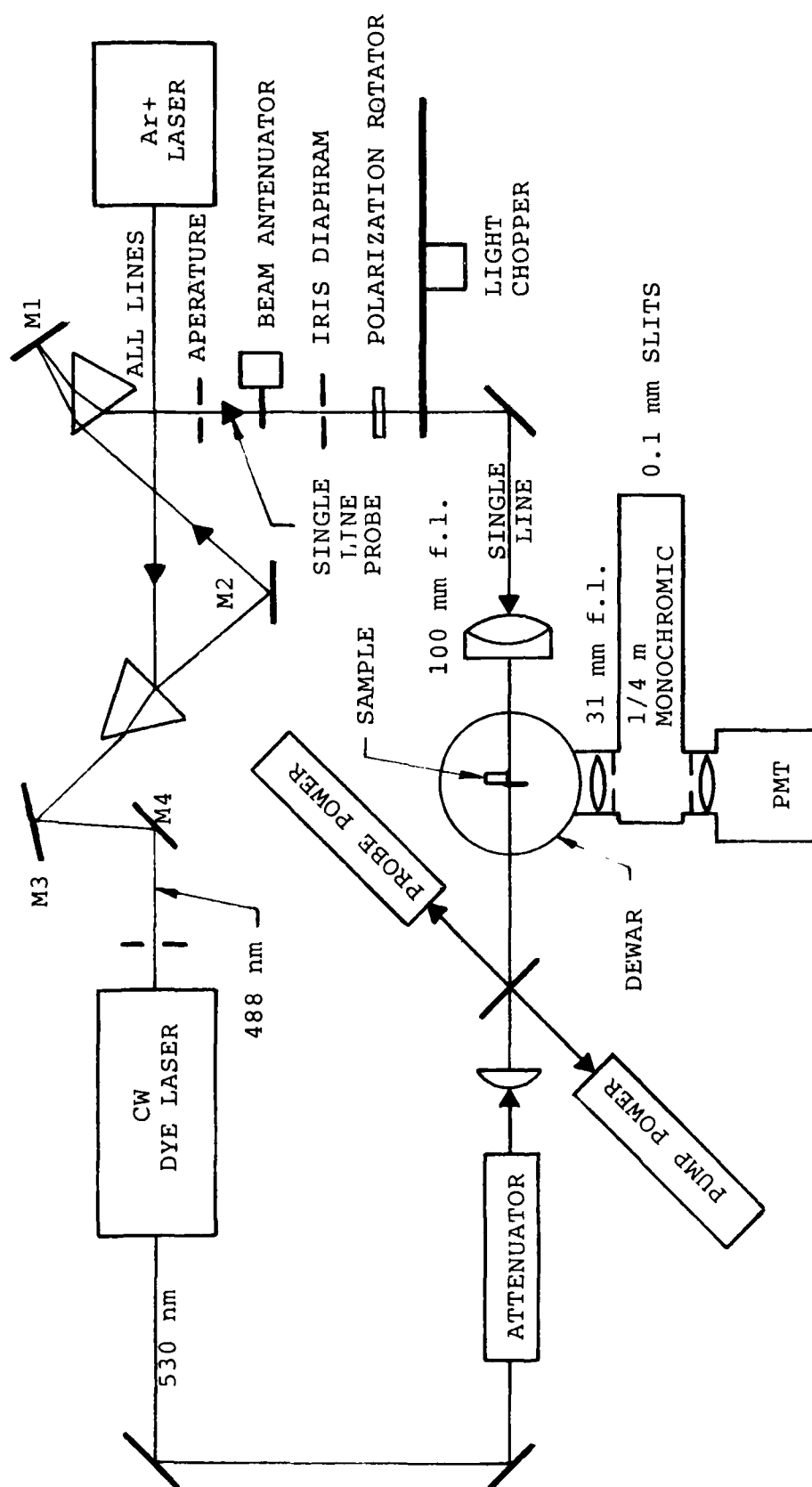
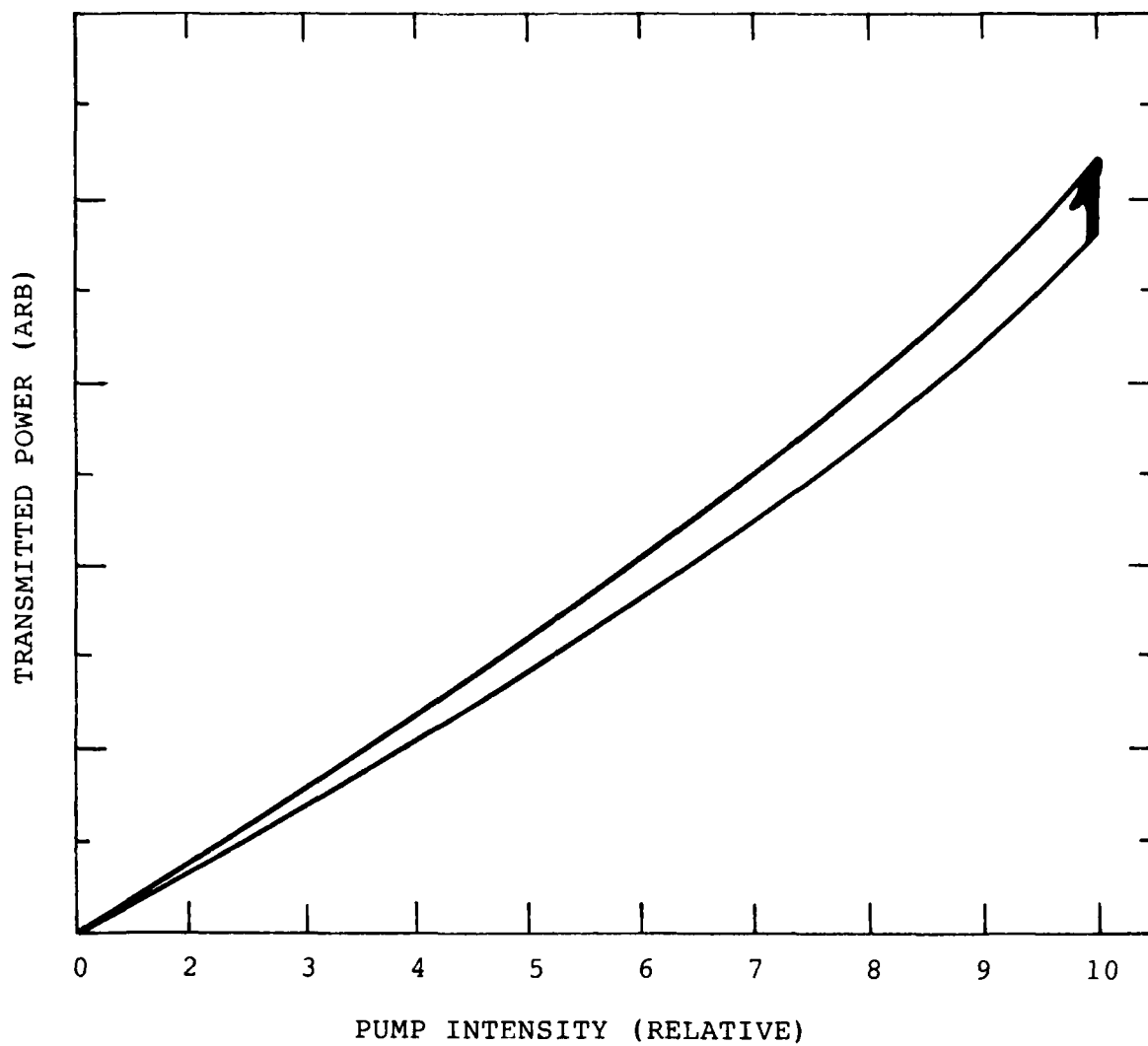Figure 3-12. Modulated Population Experiment

Figure 3-13. Avalanche Hysteresis

thermal effect; that is, as $^3H_5$ population and absorption build, the temperature in the region about the laser beam focus begins to increase, causing broadening of the absorption line. Absorption of the laser beam falls with increasing temperature.

3.3.4 Transversly Excited Laser

Several transversly excited (TE) laser experiments were attempted. The pump beam was focused by several combinations of spherical and cylindrical lenses in order to give a variety of gain region diameters and intensity levels. A list of the different crystals used is given in Table 3-2. The π and σ symbols denote the orientation of the optic axis to the Brewster surfaces, i.e., whether the π or σ line emission exits the crystal at Brewster's angle.

All attempts at laser action during this program were unsuccessful. Exceptional and diverse methods were employed to tune the three element cavity but to no avail. The output from the three mirror cavity is compared with previous results in Figure 3-14. The features near 5.0 μm from the three element cavity were found to be third order 1.6 μm features as can be inferred from the data shown in Figure 3-15. Here a 3-5 μm filter, b) and a 2-4 μm filter, c) are inserted in front of the detector while scanning the monochrometer over the feature.

Evidence for a population inversion was lacking throughout these experiments. However, a last effort reestablished the existence of a gain region. The lens and output coupler were removed. A cylindrical excitation region was focused on the side of crystal A-33. A weak beam was located on axis. The fluorescence signal was monitored by a detector as the detector was scanned vertically and horizontally to the optical table normal to the emission axis. Alignment of the mirror adjacent to the crystal causes the beam to become more collimated. These results are similar to those obtained during the previous contract (Figure 3-16) and are consistent with fluorescent output from a cylindrical gain region.
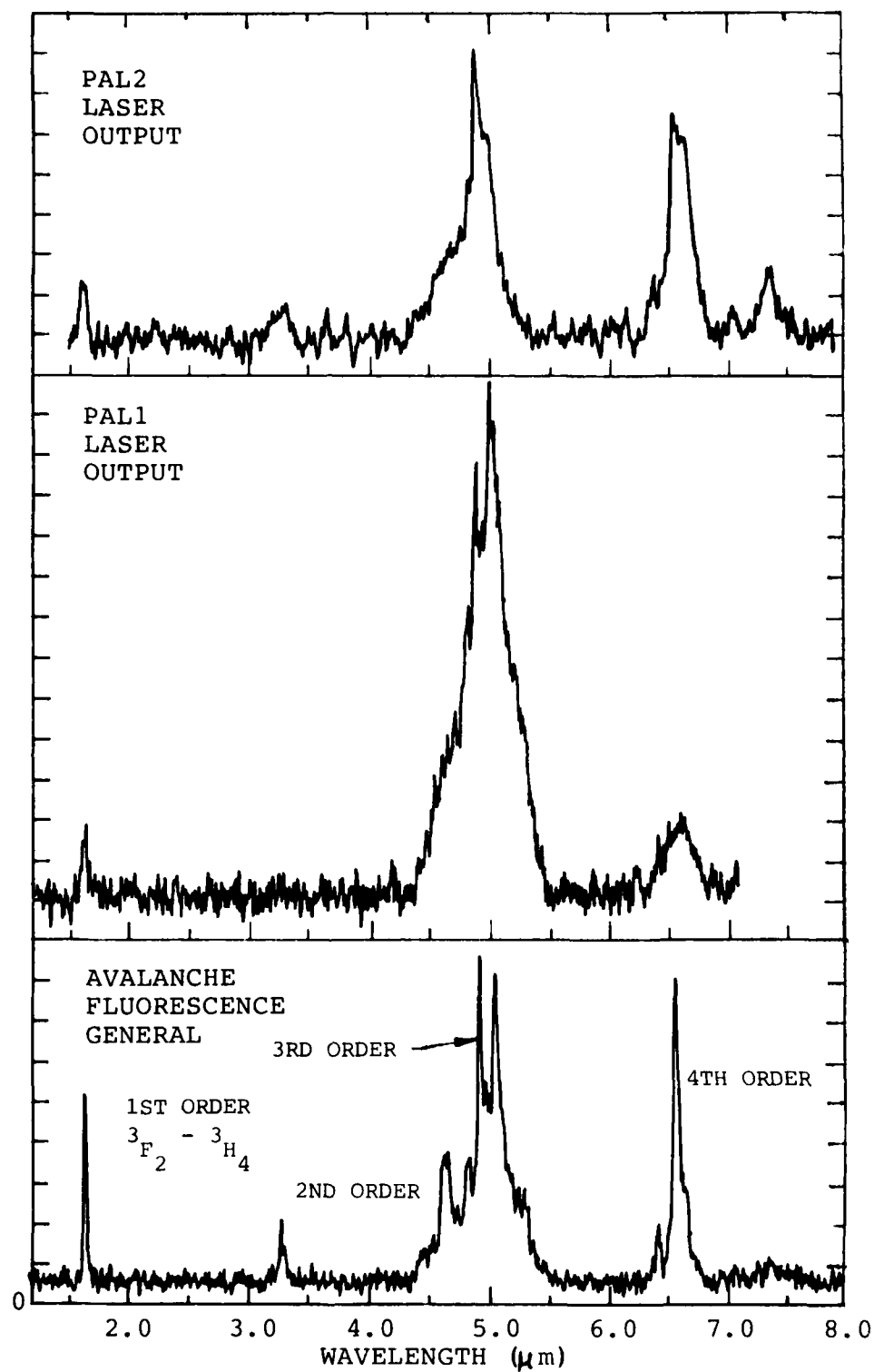
Figure 3-14.   Avalanche Laser Output
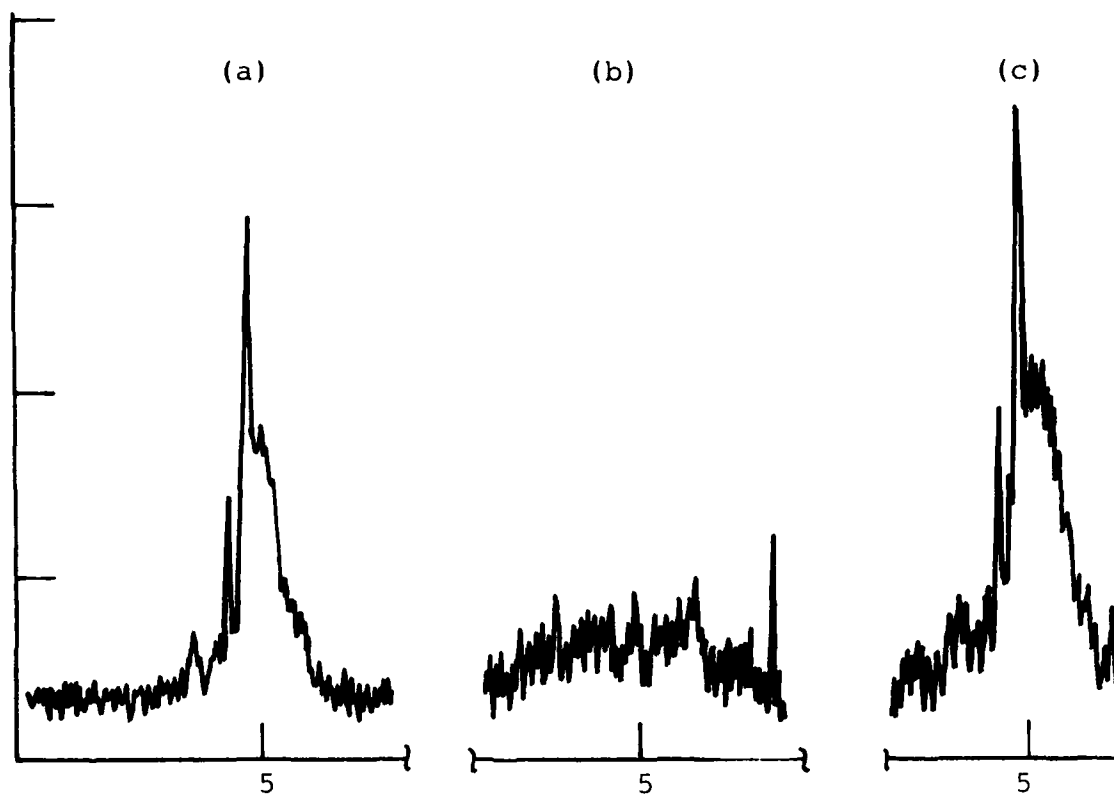
56

Figure 3-15.   Spectral Feature at 5 um Analyzed with Various Spectral
              Filters a) Unfiltered, b) 4-5 um Filter, (c)   1-3 um
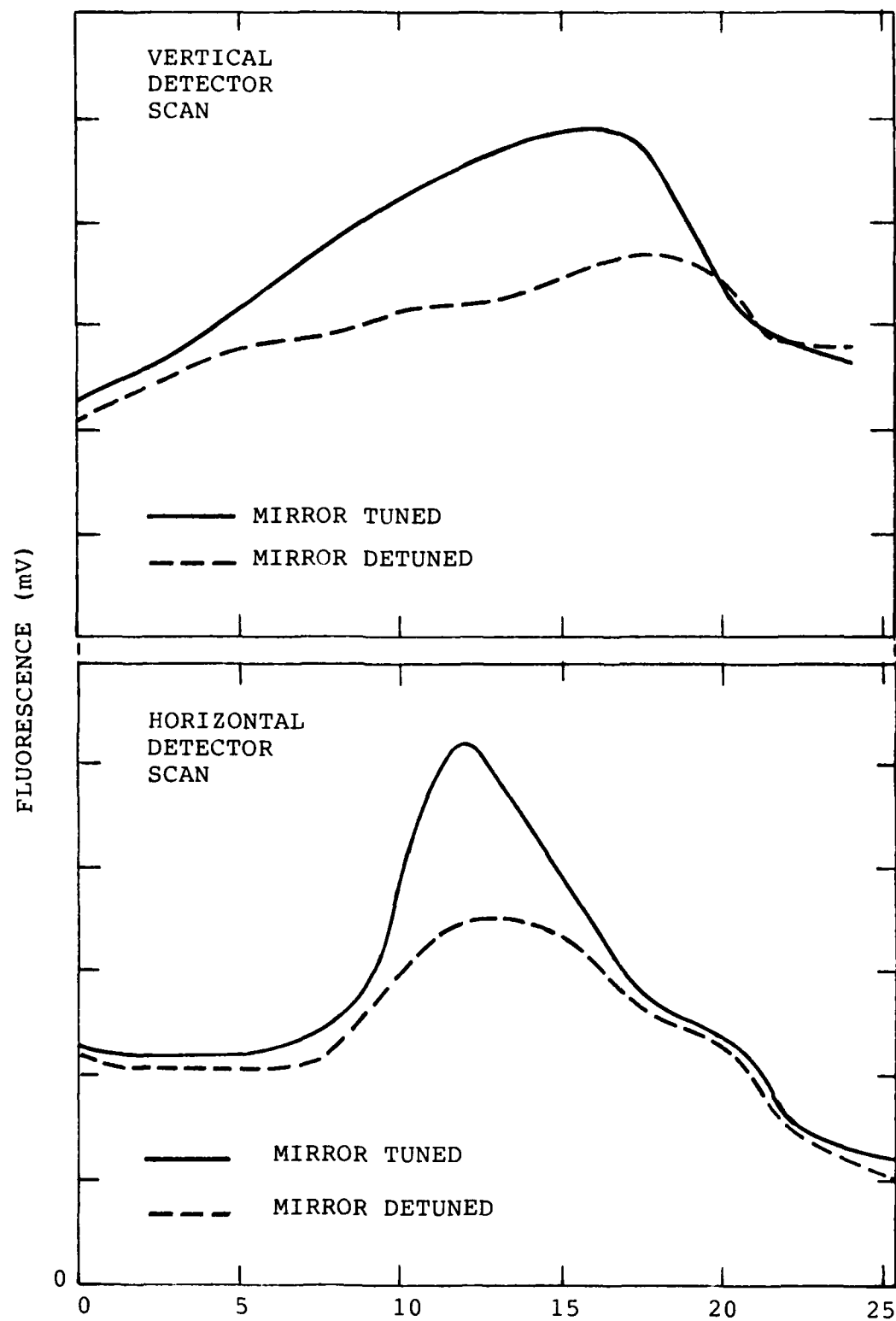   Filter

Figure 3-16. Avalanche Filament Beam Profile

3.3.5 Axially (Longitudinally) Excited Laser

The axially excited laser results were also negative. A new low tempera-
ture dewar was used for these experiments. This device, purchased from MMR
corporation, is cooled by a Joule-Thompson refrigerator. Primary advantages
are that the sample can be loaded into the dewar (not a transfer sample cell)
in the drybox, cooled within 20 minutes as opposed to overnight, and vacuum
integrity quickly assessed. Experimental difficulties with the original
research dewar persisted throughout the present program. The new dewar
promises to vastly simplify the experimental procedure in future experiments.

The axially pumped laser is shown in Figure 3-17 The intercavity lens was
optional. A list of the crystals used is given in Table 3-2. Note the differ-
ence in cycle time for this effort as compared to the transverse geometry
laser.

3.3.6 Visable Spectrum and Critical Power Measurements

The experiments described above exhausted the time available under the
contract. A short effort to look for potential problems with the new crystals
was undertaken next. A potential problem was uncovered upon examination of the
visible spectra. The experimental setup was designed to collect light from the
avalanche emitted back in the direction of the pump beam from the crystal sur-
face. In this way the fluorescent light was to transverse a minimal region of
unpumped crystal. The experimental arrangement is as shown in Figure 3-18. In
Figure 3-19 current results on crystal B-14 are compared with a similar
experiment conducted on A-33 during the previous program. The emission from
$^3P_0$ to the ground state, $^3H_4$, relative to $^3P_0 \rightarrow {}^3F_2$ or $^3H_6$ emission is much
greater for B-14 than A-33. The weakness of this emission in A-33 was the
subject of some discussion in the final report for the first program, since the
result did not agree with data from previous experiments.

The strong emission to the ground state might explain the apparent lack of
laser action in crystals presently grown. Fluorescence versus pump power were
measured next to determine if the critical pump intensity was higher for B-14
than A-33. A plot of red fluorescence versus pump power is given in Figure
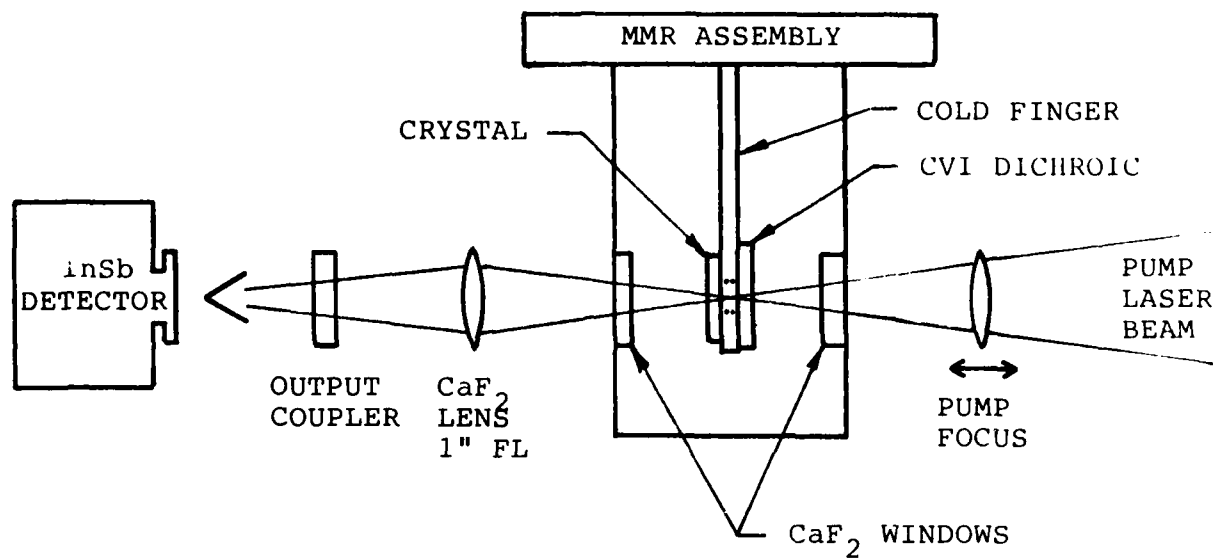3-20. The value of critical pump intensity is nearly the same for both

59

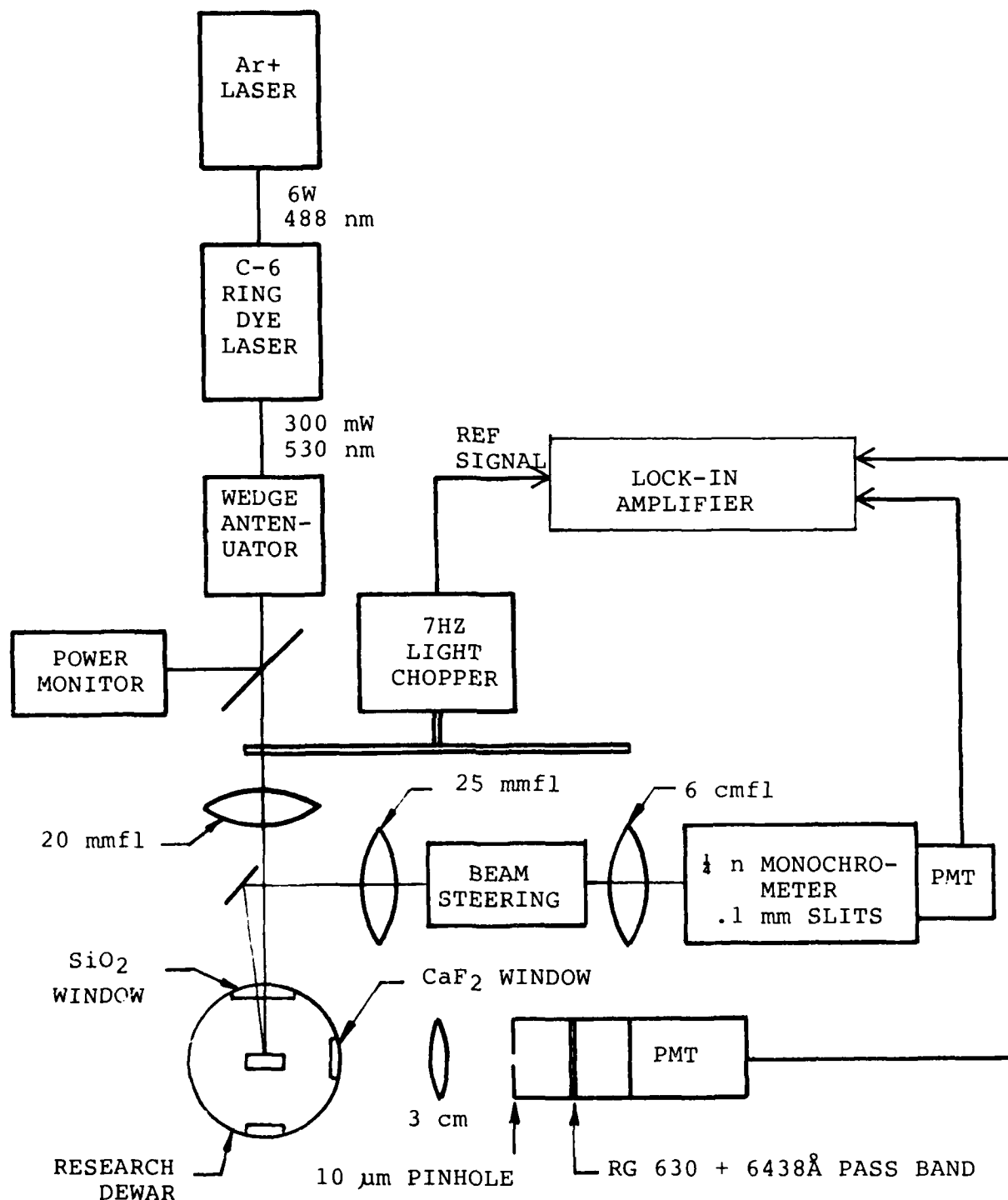Figure 3-17. Longitudinal Laser Configuration

Figure 3-18. Avalanche Spectra and Critical Power Apparatus

crystals and consistent with the values found during the first contract.

TABLE 3-9.   LASER EXPERIMENTS

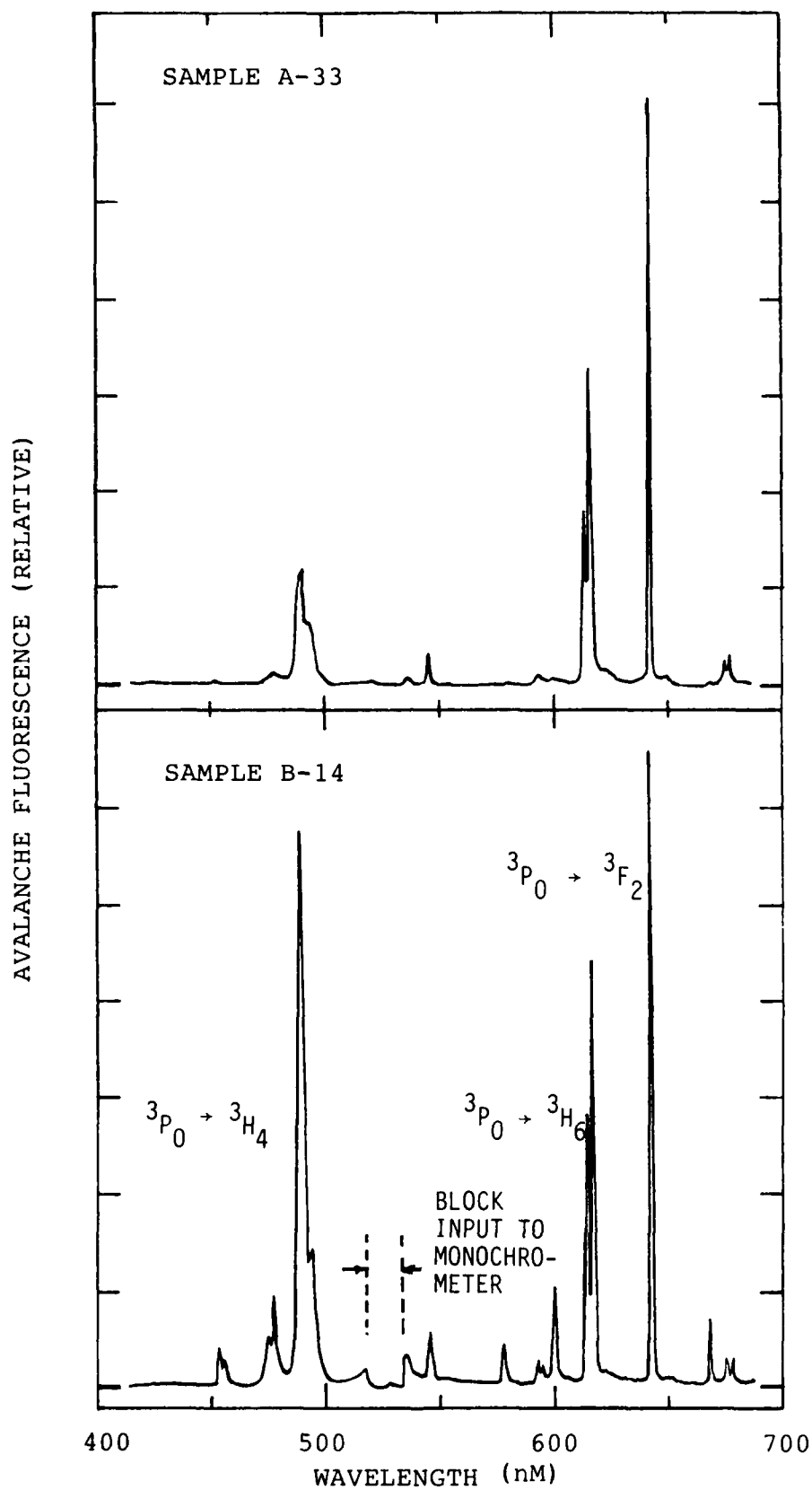| LASER TYPE	CRYSTAL	CRYSTAL THICKNESS (mm)	Pr % Mol	Date
TE π	A33	1.63	3.82	10-01-84
TE π	A33	1.35	3.82	10-13-84
TE π	B14	1.78	5.2	11-27-84
TE σ	B14	1.93	5.2	11-27-84
LE π/σ	B14	0.64	5.2	10-24-84
LE π/σ	B30	0.64	2.66	10-25-84
LE π/σ	B45	0.64	2.75	10-26-84
LE π/σ	B45	1.24	2.75	10-27-84

Figure 3-19. Visable Photon Avalanche Fluorescence,
Pump Laser Tuned to π 529.2 nm, Fluorescence
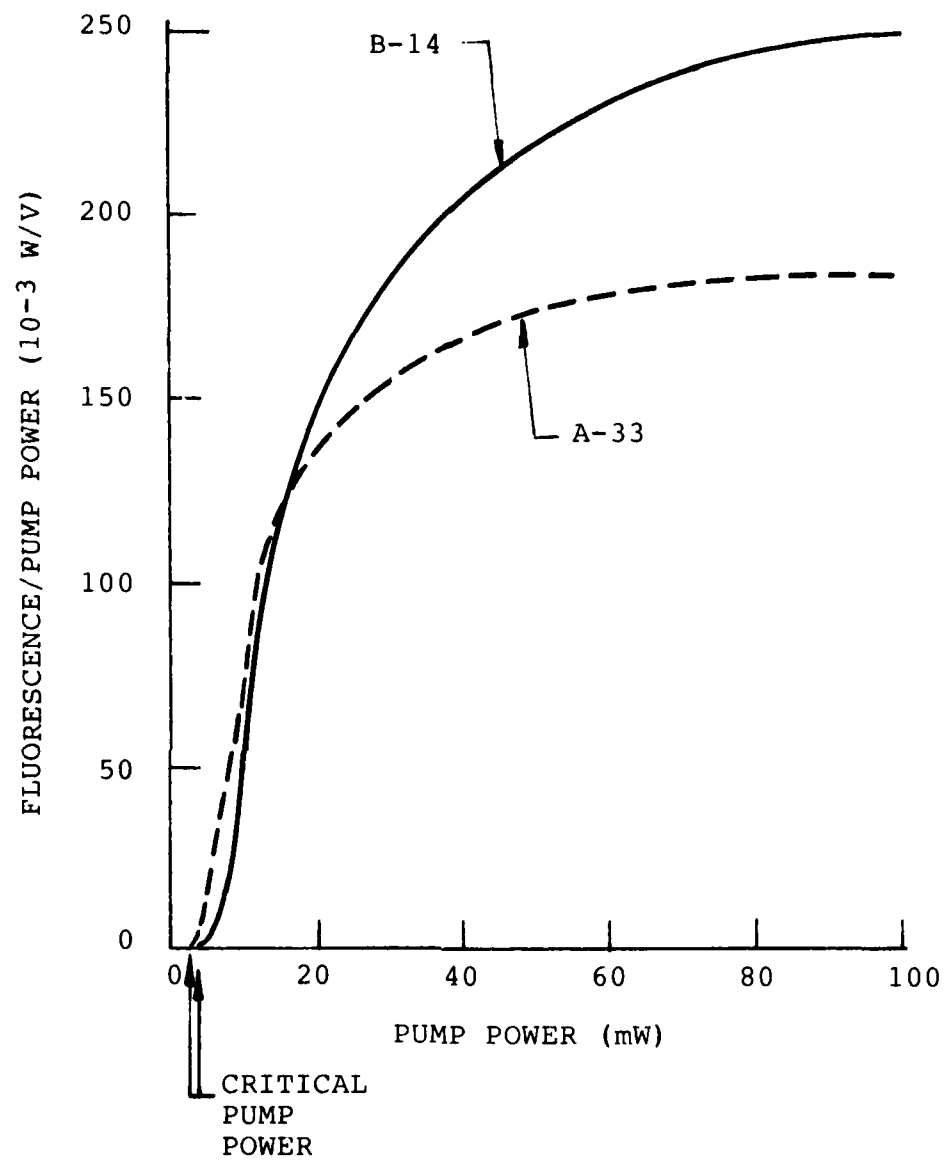from Pump Line Blocked

Figure 3-20. Red Fluorescence versus Pump Power,
200 mm Pump Lens Focal Length

64

crystals and consistent with the values found during the first contract.

TABLE 3-9. LASER EXPERIMENTS

LASER TYPE	CRYSTAL	CRYSTAL THICKNESS (mm)	Pr % Mol	Date
TE π	A33	1.63	3.82	10-01-84
TE π	A33	1.35	3.82	10-13-84
TE π	B14	1.78	5.2	11-27-84
TE σ	B14	1.93	5.2	11-27-84
LE π/σ	B14	0.64	5.2	10-24-84
LE π/σ	B30	0.64	2.66	10-25-84
LE π/σ	B45	0.64	2.75	10-26-84
LE π/σ	B45	1.24	2.75	10-27-84

4.0 DISCUSSION

In December 1982 the Pr based photon avalanche laser was successfully demonstrated. This occured at the end of a program initiated primarily to determine if laser action was even possible. Subsequently, a contract supporting an extension of the work was sought. The purpose of the extension was simply to enhance laser performance using results and experience established during the first program. However, over a year passed between conclusion of the first program and the inception of the second. During this time, the crystal growth facility was not used and the experimental set-ups described in earlier sections had to be reestablished.

Improvement of photon avalanche laser performance was to be accomplished by redesign of the laser cavity and then varing key parameters of the original laser system in order to achieve a close match between cavity and laser mode parameters. In fact, lasing action was not repeated in a limited number of attempts. The most likely reasons are deterioration of the original laser crystal due to either bulk crystal degradation or progressively smaller and more inadequate gain length caused by a polishing step in the experimental sequence. In addition to problems with the original crystal, other events limited the time available for experimental work, namely an uncontrolled crystal contamination problem and overall crystal production problems.

In spite of a failure to achieve laser performance improvement some very positive results were obtained with respect to crystal growth technology and experimental improvements. These are:

- A major improvement in the yield of the crystal production process due to optimization of the cooldown temperature gradient in the Bridgeman process.

- Discovery of LaOCl contamination and the development of a new high purity crystal production process.

- Incorporation of a new Joule-Thompson cryostat for much shorter experiment preparation times coupled with simplier and more reliable experimental arrangements.

- Development of the three miror cavity.

Experimental results include two positive features. First, observation of beam narrowing indicates gain at 4-5 μm even for a crystal which did not exhibit cavity laser action. Second, the spectral shift observed in the visible spectra for the two different crystals may provide the reason for inconsistent results in the past. The shift is likely due to variable LaOCl contamination.

In conclusion, difficulties with crystal production and crystal impurities, delays, coupled with a long experimental cycle and failure of the original crystal sample precluded observation of an increase in laser output. However, improvements in the experimental setup and crystal production process, as well as the added insights afforded by the discovery of sample dependant spectra, give clear indication of the course for future experimentation. In the near term, work (funded internally) will continue towards implementation of the new production process. We will seek quantitative verification of the photon avalanche model as well as an explanation for the weak laser output. It is hoped that future insights will suggest a strategy for taking advantage of a dramatic population inversion present in the photon avalanche driven Pr system.

5.0 REFERENCES

1. J. S. Chivian, W. E. Case, D. D. Eden, Appl. Phys. Lett, $\underline{35}$(2), 124, 1979.

2. "The Photon Avalanche in a Pr^{3+}-Based Infrared Quantum Counter," ATC Report No. B-94100/7TR-14, June 1977.

3. "Proposed Model for the Avalanche Phenomenon in Pr^{3+}," ATC Report No. B-94100/7TR-13, June 1977.

4. Unpublished results.

5. G. H. Dieke, "Spectra and Energy Levels of Rare Earth Ions in Crystals," John Wiley/Interscience, New York, 1968.

6. D. E. Cox, F. K. Fong, J. of Crys. Growth, North Holland Publishing Co., 233, 1973.

7. J. D. Corbett, Inorg. Nucl. Chem. Lett, Pergamon Press, $\underline{8}$, 337, 1972.